UCLouvain

AGRO LOUVAIN

Faculté des bioingénieurs

Methane-arrested anaerobic fermentation of orange peel waste: impact of headspace gas composition and nitrogenous co-substrates on carboxylate profiles

Auteur : Mathis Herbin

Promoteur : Prof. Patrick Gerin
Doctorante : Evelin Arcos Tigse
Lecteurs : Patrick Gerin
Benoît Stenuit
Michel Ghislain

Année académique 2025-2026

Mémoire de fin d'études présenté en vue de l'obtention du diplôme de
Bioingénieur : chimie et bio-industries

Acknowledgement

First and foremost, I would like to express my sincere gratitude to my supervisor, Patrick Gerin, for agreeing to guide me throughout this research project, which has spanned nearly two years.

I would also like to warmly thank Evelin Arcos Tigse for her constant supervision and for everything she taught me throughout my master's thesis.

My thanks go to Benoît Stenuit for his valuable advice regarding presentations and for taking the time to explain several experimental procedures.

A special thank you to Thomas Nicolay, who was very present during the first year and from whom I learned an immense amount.

I am also grateful to Alexandre Jolly for his patience in teaching me experimental protocols.

I would like to extend my appreciation to the three thesis reviewers for the time and attention they will dedicate to reading and evaluating this work.

Finally, I want to thank my family for their unwavering support and encouragement throughout my entire university journey.

Contributor Roles Taxonomy

	Mathis Herbin	Other contributors	Artificial Intelligence
Conceptualization	**YES**	**Prof. Patrick Gerin**	
Methodology	**NO**	**Prof. Patrick Gerin, Evelin Arcos Tigse**	
Investigation	**YES**	**Evelin Arcos Tigse**	**Gemini (to search articles and extract information)**
Formal analysis	**YES**	**Thomas Nicolay**	**Gemini (calculation, synthetise, analyse)**
Validation	**YES**	**Prof. Patrick Gerin**	
Writing – original draft	**YES**		**Gemini (guide, reformulation, coherence checking), Deepl (traduction)**
Writing – review & editing	**YES**	**Prof. Patrick Gerin**	
Visualization	**YES**		**Gemini (help to construct graph)**
Supervision	**NO**	**Prof. Patrick Gerin, Evelin Arcos Tigse, Thomas Nicolay**	

List of abbreviations

4-MV
4-Methylvalerate (Internal Standard)
AD
Anaerobic Digestion
ATP
Adenosine Triphosphate
BESA
2-Bromoethanesulfonic Acid
C/N
Carbon-to-Nitrogen Ratio
C2
Acetic Acid / Acetate
C3
Propionic Acid / Propionate
C4
Butyric Acid / Butanoate / Butyrate
C5
Valeric Acid / Valerate
C6
Caproic Acid / Caproate / Hexanoic Acid
C7
Heptanoic Acid / Heptanoate
C8
Caprylic Acid / Caprylate / Octanoic Acid
CAPEX
Capital Expenditure
CNG
Compressed Natural Gas
CoA
Coenzyme A
COD
Chemical Oxygen Demand
DNA
Deoxyribonucleic Acid
EEO
Excessive Ethanol Oxidation
Fd_{red}
Reduced Ferredoxin
FID
Flame Ionization Detector
FW
Fresh Weight
GC
Gas Chromatography

GC-FID
Gas Chromatography – Flame Ionization Detection
GC-TCD
Gas Chromatography – Thermal Conductivity Detection
HHV
Higher Heating Value
HRC
High-Yield Recovery Column
LNG
Liquefied Natural Gas
MCCA
Medium-Chain Carboxylic Acid
MCFA
Medium-Chain Fatty Acid
ML
Mixed Liquor
NADH/NAD$^+$
Nicotinamide Adenine Dinucleotide (Oxidized / Reduced form)
OPEX
Operational Expenditure
PCR
Polymerase Chain Reaction
PMF
Proton-Motive Force
PTFE
Polytetrafluoroethylene
PVC
Polyvinyl Chloride
RAS
Return Activated Sludge
rBOX
Reverse β-Oxidation
ROS
Reactive Oxygen Species
SAF
Sustainable Aviation Fuels
SCCA
Short-Chain Carboxylic Acid
SCFA
Short-Chain Fatty Acid
SSCF
Simultaneous Saccharification and Co-Fermentation
TCD
Thermal Conductivity Detector
THF
Tetrahydrofolate
TS

Total Solids
USD
United States Dollar
VFA
Volatile Fatty Acid
VS
Volatile Solids
WWTP
Wastewater Treatment Plant

Table of contents

1 Introduction

In the face of depleting fossil resources and the urgent climate crisis, our industrial models are undergoing a major systemic transformation. The transition toward a circular bioeconomy has now become a global strategic imperative. Within this paradigm, biomass and organic byproducts are no longer viewed as mere waste to be disposed of, but rather as renewable resources with high valorisation potential. In bioprocess engineering, a fundamental shift is progressively taking place: the evolution from the classic "Waste-to-Energy" concept (focused on biomethane production through conventional anaerobic digestion) toward a "Waste-to-Chemicals" model. This is embodied by the carboxylate platform, which aims to interrupt the anaerobic trophic cascade to produce high-value chemical building blocks.

Among the target metabolites of this platform, medium-chain carboxylic acids (MCCAs), such as caproic acid (C6), are generating significant scientific and industrial interest. Due to their extended carbon chain and hydrophobic nature, MCCAs exhibit low solubility in aqueous phases when protonated, which considerably facilitates their *in situ* extraction and reduces the energy footprint of downstream processing. Valued across green chemistry, sustainable aviation fuels (SAF), cosmetics, and antimicrobial additives for animal feed, MCCAs command a market value substantially higher than that of methane.

The biological production of MCCAs relies on chain elongation via the reverse β-oxidation (rBOX) pathway, carried out by strict anaerobic microbial consortia. However, implementing this process using real organic feedstocks faces complex bioenergetic and operational hurdles. Orange peels, an abundant byproduct of the fruit juice industry, constitute a prime carbonaceous feedstock due to their high content of soluble carbohydrates and pectin. Nevertheless, their mono-digestion presents two major limitations: on the one hand, a very high carbon-to-nitrogen (C/N) ratio (> 40:1), reflecting a severe nitrogen deficiency that hinders the enzymatic synthesis of the microbiome; on the other hand, the presence of essential oils composed of over 90% D-limonene. This hydrophobic monoterpene inserts into cell membranes and exerts acute selective toxicity, particularly against methanogenic archaea. While this natural inhibition offers an opportunity to block methanogenesis without resorting to costly synthetic chemical inhibitors (such as BESA), the reversibility of the phenomenon

through D-limonene biotransformation or volatilization often allows methanogens to re-emerge, thus closing the elongation window.

To sustain MCCA production in open mixed cultures, a dual engineering strategy is required. On the one hand, the co-digestion of orange peels with malting byproducts (rootlets and green malt) allows for the addition of bioavailable organic nitrogen and essential micronutrients, thereby rebalancing the C/N ratio without risking toxic ammonia shocks. On the other hand, rigorous control of the gas phase (headspace) under strict anaerobiosis—specifically through the injection of a reducing atmosphere of hydrogen and carbon dioxide (H_2/CO_2)—provides the thermodynamic driving force required to overcome the bioenergetic barriers of rBOX and fuel homoacetogenesis.

It is at the intersection of these synergies that this master's thesis is situated. The primary objective of this research is to evaluate and optimize the anaerobic fermentation of orange peels inoculated with wastewater treatment plant sewage sludge, by studying the complex interaction between D-limonene toxicity, C/N rebalancing via malting co-substrates, and gaseous supplementation, in order to selectively steer electron fluxes toward MCCA synthesis.

2 State of the art

2.1 From anaerobic digestion to the carboxylate platform

2.1.1 Conventional anaerobic digestion and its economic limitations

The management and valorisation of residual biomass constitute a major challenge for the ecological transition and the circular economy. The Figure 1 shows the system to aim to minimize the number of biowastes through the recovery of high added value compounds, still present in the wastes. By this way, wastes are substrates for a secondary raw materials market with the creation of new jobs opportunities and economic gain. In the specific case of organic wastes, they can be also exploited for biofuels and bioenergy productions but only after the "recycling" stage. Instead, the landfill disposal and incineration of wastes should be considered as the last choice or avoided at all (Battista et al. 2020).

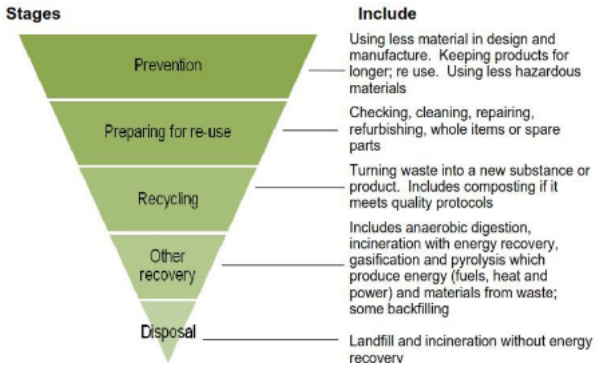

Figure 1. Pyramidal hierarchy for wastes valorisation from https://ec.europa.eu/environment/waste/framework

Historically, conventional anaerobic digestion has established itself as the reference technology for treating complex organic waste, such as sewage sludge, agricultural effluents, and agro-industrial residues (Agler et al. 2011). This bioprocess relies on a complex synergy between various microbial guilds operating in the absence of oxygen. The degradation metabolism typically occurs in four sequential steps: hydrolysis, acidogenesis, acetogenesis, and finally, methanogenesis (Figure 2). The culmination of this trophic cascade is the mineralization of organic matter into biogas; a gaseous mixture primarily composed of methane and carbon dioxide.

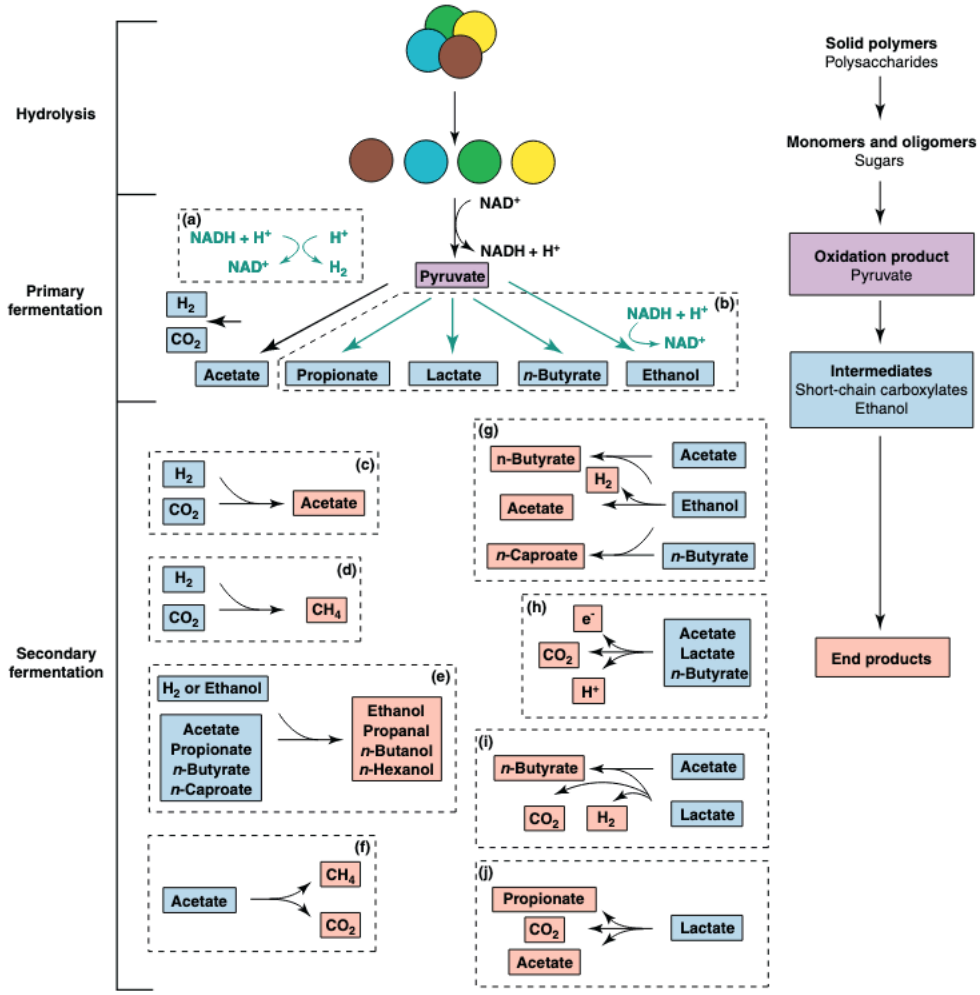

Figure 2. Hydrolysis of solid polymers to monomers and oligomers (e.g. insoluble polysaccharides, such as cellulose and hemicellulose) and subsequent conversion by primary and fermentation reactions with undefined mixed cultures. During primary fermentation of sugars, substrates are converted to pyruvate, which results in the production of NADH and H+. All equivalents must be re-oxidized via H+ reduction by: (a) NADH oxidation; or (b) NADH oxidation via reduction of pyruvate or its oxidized organic derivatives, depending upon the hydrogen partial pressure [8]. At increasing hydrogen partial pressures, the flow of electrons from NADH shifts from H2, acetate and CO2 production towards formation of increasingly reduced fermentation products [70]. CO2 and H2 are produced in the pyruvate oxidation reaction that is catalysed by pyruvate:ferredoxin oxidoreductase. The products of primary fermentation can react further within undefined mixed cultures through several secondary fermentation reactions: (c) autotrophic homoacetogenesis; (d) hydrogenotrophic methanogenesis; (e) carboxylate reduction to alcohols with hydrogen or ethanol; (f) aceticlastic methanogenesis; (g) chain elongation of carboxylates with ethanol; (h) electricigenesis (i) lactate oxidation to n-butyrate (acetate and H+ as electron acceptor); and (j) lactate reduction to propionate (oxidation to acetate for energy conservation)(Agler et al. 2011).

While anaerobic digestion is currently a mature technology widely deployed on an industrial scale for renewable energy production, its economic model increasingly faces structural challenges. The primary pitfall lies in the low added value of methane on the global energy market, coupled with its relatively low volumetric energy density compared to other energy carriers (36 MJ/m^3 for methane gas versus >25000 MJ/m^3 for liquid biofuels) (Bastidas-Oyanedel and Schmidt 2018).

Furthermore, raw biogas cannot be optimally utilized without undergoing costly purification steps known as upgrading (Figure 3). These separation processes, aimed at removing CO_2, hydrogen sulfide, siloxanes and water vapor, require heavy infrastructure that significantly undermines the overall profitability of the facilities, particularly for small-to medium-sized bioreactors (Angelidaki et al. 2018; Wasajjaa et al. 2020).

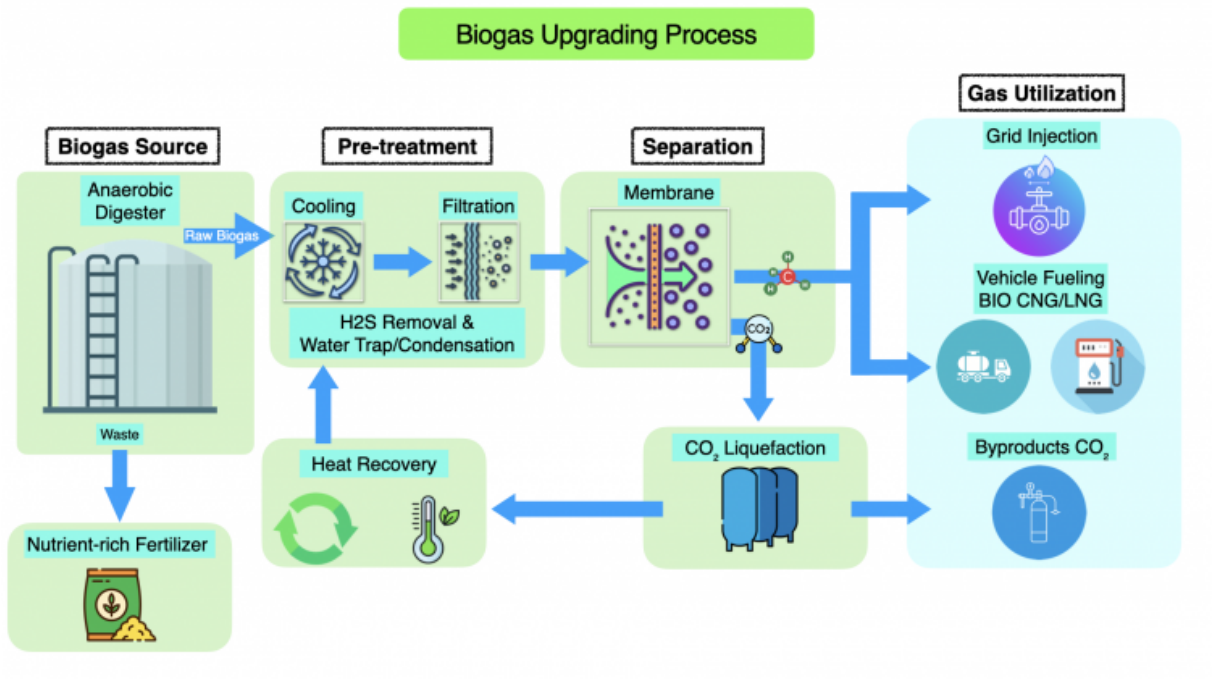

Figure 3. Biogas upgrading process (Aces Process)

Faced with these techno-economic limitations, a paradigm shift is currently taking place within the scientific and industrial community : the transition from a Waste-to-energy model to a Waste-to-chemicals model (Agler et al. 2011). In this context, bioprocess engineering aims to interrupt the anaerobic digestion chain to prevent methane production, favouring instead the accumulation of metabolic intermediates with a higher market value. The Figure 4 below shows that propionic, butyric and caproic acids are more valuable than methane.

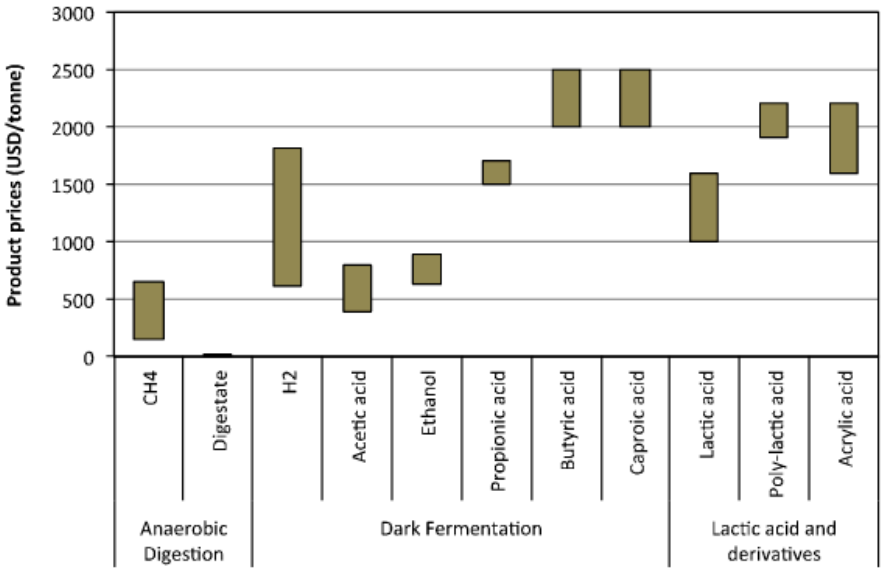

Figure 4. Market price ranges of main anaerobic-fermentation-based products (Bastidas-Oyanedel and Schmidt 2018)

To illustrate this potential, Bastidas-Oyanedel and Schmidt (2018) evaluated a regional-scale biorefinery treating 50 tonnes/day of segregated food waste, a capacity representative of commercial organic waste processing plants. Based on a typical food waste substrate containing 19% Total Solids (TS) and 16% Volatile Solids (VS), their techno-economic assessment calculated net profits after accounting for annualized capital (CAPEX) and operational (OPEX) expenditures over a 20-year project lifetime. The baseline scenario, conventional anaerobic digestion with biomethane injected into the gas grid, yielded a modest net profit of 19 USD/t_VS (3 USD/t_raw food waste). In contrast, shifting to a carboxylate platform via dark fermentation paired with downstream separation and purification of acetic and butyric acids generated a net profit of 296 USD/t_VS (47 USD/t_raw food waste). This 15-fold profit increase underscores how chemical platform recovery drastically outperforms pure energy vector production even after factoring in the substantial purification costs (Bastidas-Oyanedel and Schmidt 2018).

2.1.2 Methane-arrested fermentation

To overcome the low profitability of the biogas sector, bioprocess engineering has developed the concept of « methane-arrested anaerobic digestion », often associated with dark fermentation within the framework of the carboxylate platform (Henry et al. 2023a). Unlike

conventional digestion, this approach aims to intentionally decouple the trophic cascade. The operational objective is to suppress, or at least severely inhibit, the activity of methanogenic archaea, thereby preventing the conversion of metabolic intermediates into methane, which normally act as the terminal electron sink of the system.

In the absence of active methanogenesis, carbon and electron fluxes are redirected. The metabolic products generated during the hydrolysis, acidogenesis and acetogenesis phases, accumulate transiently or permanently in the bioreactor. The fermentation broth thus becomes massively enriched in short-chain carboxylic acids (SCCAs). The metabolic profile of this primary acidogenic fermentation is predominantly dominated by acetic acid (C2), propionic acid (C3) and butyric acid (C4), with the exact proportions depending heavily on the stoichiometric composition of the initial substrate and the environmental conditions (Agler et al. 2011). Maintaining this accumulation is a technical challenge that traditionally requires strict control of the bioreactor parameters to prevent the adaptation and proliferation of resilient methanogens.

Within the overall architecture of the carboxylate platform, this arrested fermentation step is fundamental. The accumulation of SCCAs and more specifically the pool of acetate generated from complex biomass, is not an end in itself. These highly soluble molecules will act as essential electron acceptors and building blocks to trigger the subsequent phase: chain elongation. Biochemically, acetate operates as the core molecular primer that captures the reducing equivalents derived from the electron donor, shifting the system's focus from simple carbon degradation to the synthesis of longer, hydrophobic molecules (Agler et al. 2011).

2.1.3 Medium-chain carboxylic acids: physicochemical advantages, market value, and thermodynamic superiority

Although the SCCAs accumulation is a crucial first step in methane-arrested fermentation, the economic viability of SCCAs as end products remains severely hindered by downstream processing. Molecules such as acetate or propionate are highly hydrophilic and water-soluble. Their recovery from the dilute fermentation broth, a stage known as downstream processing, which encompasses all unit operations required to isolate, purify, and concentrate the target bioproduct, requires energy-intensive processes, such as azeotropic distillation, liquid-liquid

extraction with low distribution coefficients, or electrodialysis. These thermal and mechanical recovery steps often negate the economic and ecological benefits of their biological production (Agler et al. 2011).

To bypass these downstream bottlenecks, chain elongation has emerged as the central biochemical process of the carboxylate platform. Through reverse β-oxidation (rBOX), SCCAs acting as electron acceptors are condensed with an electron donor to synthetise MCCAs typically comprising carbon chains of 6 to 12 atoms, most notably caproic acid (C6) and caprylic acid (C8). Regardless of whether reducing power is supplied by organic co-substrates or inorganic gaseous donors like hydrogen, the metabolic pathway drives the sequential addition of two-carbon (C2) units onto short-chain primers, as summarized by the general stoichiometry:

$$R - COO^- + CH_3CH_2OH \rightarrow R - CH_2CH_2COO^-$$

The lengthening of the carbon chain provides MCCA recovery with two major industrial advantages over SCCA harvesting:

The addition of hydrophobic methylene (-CH2-) groups drastically decreases the aqueous solubility of the molecule. Under acidic conditions, the uncharged, protonated form (n-caproic acid) reaches a low solubility limit (~10.8 g/L at 20°C). This enables cost-effective, low-energy *in situ* phase separation techniques such as membrane pertraction or liquid-liquid extraction. Continuous *in situ* product extraction is particularly critical because accumulating protonated MCCAs cross bacterial cell membranes, causing intracellular acidification, dissipation of the proton-motive force, and cell lysis (Agler et al. 2011). From a market perspective, MCCAs command a significantly higher market price than methane or SCCAs, as established previously (Bastidas-Oyanedel and Schmidt 2018).

Caproic acid is a highly versatile platform chemical. It finds direct applications as an antimicrobial additive in the food and animal feed industries, replacing growth-promoting antibiotics. Furthermore, through downstream chemical conversion processes, MCCAs can be transformed into bioplastics, green solvents, fragrances, or even « drop-in » biofuels for the aviation industry (Liu et al. 2025). The transition from biogas production to MCCA synthesis

therefore fully justifies the engineering efforts required to control these mixed microbial cultures.

The architectural superiority of the carboxylate platform is fundamentally grounded in its thermodynamic efficiency. Comparative mass and energy balances demonstrate that the biological conversion step toward carboxylic acids achieves a theoretical energy efficiency exceeding 93% (defined as the ratio of the higher heating value (HHV) of the produced carboxylates to that of the polysaccharide feedstock).

Furthermore, experimental data establish that the carboxylate platform significantly outperforms competing technologies, achieving up to 72.6% of its theoretical maximum alcohol yield (expressed as ethanol equivalents per ton of dry biomass), compared to barely 55% for conventional thermochemical conversion or simultaneous saccharification and co-fermentation (SSCF). Finally, when an external source of hydrogen (e.g., renewable electrolysis) is supplied to reduce all available biomass carbon into liquid fuel, theoretical ethanol yields increase by 65% for biological platforms (expanding from 175 to 289 gal/ton of dry biomass), underscoring the necessity of strict gas-phase management in open-culture microbiomes (Holtzapple and Granda 2009).

2.2 Chain elongation via reverse β-oxidation

2.2.1 Metabolic pathway and microbial actors

Microbial chain elongation within the carboxylate platform primarily relies on the reverse β-oxidation, or rBOX, metabolic pathway (Figure 5). Unlike classical β-oxidation in eukaryotes, wich is an oxidative, catabolic pathway dedicated to fatty acid degradation and energy harvesting, rBOX operates in the opposite thermodynamic direction: it is a reductive, anabolic, and cyclic anaerobic pathway. This pathway enables specific functional guilds of bacteria (such as *Clostridium kluyveri*) to elongate the carbon chain of SCCAs by sequentially adding two carbon units (Angenent et al. 2016)

From a biochemical perspective, initiating an rBOX cycle requires the interaction of two distinct chemical inputs: a carboxylate primer acting as an electron acceptor (typically acetate or propionate derived from primary acidogenesis) and a reduced substrate acting as both the primary electron and carbon donor (predominantly ethanol or lactate). The partial intracellular oxidation of this primary substrate yields the essential C_2 elongation building block (acetyl-CoA) alongside the reducing equivalents (NADH and reduced ferredoxin, Fd_{red}) required to drive the reductive steps.

Each intracellular enzymatic cycle proceeds through four successive catalytic steps: (1) condensation of acetyl-CoA with the acyl-CoA primer to extend the chain by two carbons (mediated by a thiolase), (2) a first reduction of the resulting β-ketoacyl-CoA to a β-hydroxyacyl-CoA using NADH (mediated by a β-hydroxybutyryl-CoA dehydrogenase), (3) dehydration to yield an enoyl-CoA (mediated by a crotonase), and (4) a second, terminal reduction of the double bond using NADH and reduced ferredoxin to yield an elongated acyl-CoA (mediated by a butyryl-CoA dehydrogenase complex) (Spirito et al. 2014).

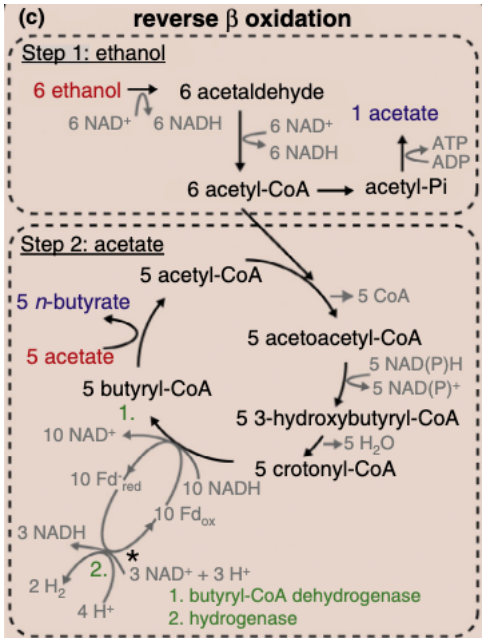

Figure 5. Reverse β-oxidation (Spirito et al. 2014)

At the end of this four-step catalytic cycle, the carbon chain of the primer is extended by two carbon atoms. The resulting elongated intermediate (e.g., butyryl-CoA) can follow two distinct metabolic fates: it can either be cleaved by a CoA-transferase to release the free carboxylate (e.g., butyrate) into the extracellular medium, or serve as a new primer to re-enter the rBOX

cycle for additional rounds of C_2 extension, producing caproate or caprylate (Agler et al. 2011). This sequential re-entry into the catalytic loop explains the time-dependent evolution (or dynamic shift) of the product spectrum observed during fermentation. Rather than yielding a fixed end-product, the carboxylate profile dynamically transitions over time from short-chain precursors (C_2) to intermediate (C_4) and longer-chain carboxylates (C_6-C_8), as accumulating shorter carboxylates progressively serve as primers for higher-order elongation (Grootscholten et al. 2014).

Microbiologically, species capable of catalysing this pathway predominantly belong to the phylum *Bacillota*. The historical biological model, originally isolated, is *Clostridium kluyveri*, a bacterium capable of converting ethanol and acetate into butyrate and caproate (Seedorf et al. 2008). However, within open and complex mixed cultures, such as those found in industrial bioprocesses, chain elongation is often driven by a much broader diversity of microorganisms some of which are presented below in Table 1, including genera such as *Megasphaera* or *Caproiciproducens (Zhang et al. 2026)*.

Table 1. Isolated bacterial strains known to produce MCCAs (Stamatopoulou et al. 2020)

Name	Isolation Source	Substrates	Products
Clostridium kluyveri	Canal mud	Glucose, Fructose, Sorbitol, Mannitol, Lactate, Pyruvate, Serine, Formate	C4, C5, Ethyl crotonate, C6, C7, C8, CO_2 and H_2
Megasphaera elsdenii	Sheep rumen	Glucose, Fructose, Maltose, Mannitol, Sorbitol, Lactate	C2, C3, C4, C5, C6, CO_2 and H_2
Ruminococcaceae bacterium CPB6	Fermentation pit	Lactate, Ethanol, Glucose	C4, C6
Caproiciproducens galactitolivorans BS-1	Wastewater treatment plant	Galactitol, C2	Ethanol, Butanol, C2, C4, C6, H_2
Eubacterium limosum	Pea-blanching wastes	H_2 and CO_2	C2, C4, C5, C6
Eubacterium pyruvativorans	Sheep rumen	Formate, Acetate, Propionate, iso-butyrate, C4, Lactate	C4, C5, C6
Rhodospirillum rubrum	Dead mouse	Glucose, Fructose, Sucrose, CO	C6
Pseudoramibacter alactolyticus	Lung abscess	Glucose	Formate, C2, C4, C5, C6, C8
Megasphaera hexanoica	Cow rumen	Fructose, Mannose	C2, iso-butyrate, iso-valerate, C6, H_2, CO_2, H_2S
Clostridium sp. BL-3	Anaerobic bioreactor	Lactate, Ethanol, Xylose, Fructose	C2, C4, iso-butyrate, C6
Clostridium sp. BL-4	Anaerobic bioreactor	Lactate, Ethanol, Xylose, Fructose	C2, C4, iso-butyrate, C6
Clostridium sp. BL-6	Anaerobic bioreactor	Lactate, Ethanol, Xylose, Fructose	C2, C4, iso-butyrate, C6
Caproiciproducens sp. 7D4C2	Open-culture, chain-elongating bioreactor	Glucose, Fructose	Lactate, C2, C4, C6, H_2, CO_2

2.2.2 Thermodynamic barriers to carbon chain elongation

Although the enzymatic machinery for rBOX is present within the microbiome, chain elongation faces a fundamental constraint: the thermodynamic barrier. From a bioenergetic standpoint, the addition of carbon units to form medium-chain acids is a highly reductive process. It requires not only carbon but, more importantly, a massive input of energy and reducing equivalents. In standard ethanol-driven models, this thermodynamic hurdle is overcome through metabolic coupling, yielding global Gibbs free energy changes ($\Delta G_r°'$) at 37°C of -194.46 kJ/mol for the conversion of acetate to n-butyrate, and -182.78 kJ/mol for the further elongation of n-butyrate into n-caproate, as we can see in Table 2 (Agler et al. 2011).

Table 2. Secondary fermentation reaction and processes (Agler et al. 2011)

Reaction	Microbe	Carboxylate conversion reactions	Coupled repetitions[d]	$\Delta G_r^{o'}$ (kJ/mol at 37 °C)[e]	$\Delta G_r^{o'}$ (kJ/mol at 55 °C)[e]
(c) Carbon dioxide reduction to acetate	*Acetobacterium woodii*	$4H_2 + 2CO_2 \rightarrow acetate^- + H^+ + 2H_2O$		−86.78	−74.56
(d) Hydrogenotrophic methanogenesis	*Methanospirillum hungatei*	$4H_2 + CO_2 \rightarrow CH_4 + 2H_2O$		−125.84	−118.47
(e) Carboxylate reduction with molecular hydrogen	[b]	$acetate^- + H^+ + 2H_2 \rightarrow ethanol + H_2O$		−7.22	−4.37
		$propionate^- + H^+ + 2H_2 \rightarrow propanol + H_2O$		−7.49	−4.59
		$n\text{-butyrate}^- + H^+ + 2H_2 \rightarrow n\text{-butanol} + H_2O$		−3.58	−0.73
		$n\text{-caproate}^- + H^+ + 2H_2 \rightarrow n\text{-hexanol} + H_2O$		−7.55	−3.63
(e) Propionate reduction with ethanol	[c]	$ethanol + H_2O \rightarrow acetate^- + H^+ + 2H_2$	×1	7.22	4.37
		$propionate^- + H^+ + 2H_2 \rightarrow propanol + H_2O$	×1	−7.49	−4.59
				Total = −0.27	**Total =** −0.22
(f) Aceticlastic methanogenesis	*Methanosaeta soehngenii*	$acetate^- + H^+ \rightarrow CH_4 + CO_2$		−39.06	−43.91
(g) Chain elongation of acetate	*Clostridium kluyveri*	$ethanol + H_2O \rightarrow acetate^- + H^+ + 2H_2$	×1	7.22	4.37
		$ethanol + acetate^- \rightarrow n\text{-butyrate}^- + H_2O$	×5	−201.68	−198.50
				Total = −194.46	**Total =** −194.13
(g) Chain elongation of *n*-butyrate	*C. kluyveri*	$ethanol + H_2O \rightarrow acetate^- + H^+ + 2H_2$	×1	7.22	4.37
		$ethanol + n\text{-butyrate}^- \rightarrow n\text{-caproate}^- + H_2O$	×5	−190.00	−195.20
				Total = −182.78	**Total =** −190.83
(i) Lactate oxidation to *n*-butyrate	*Clostridium acetobutylicum*	$2\ acetate^- + H^+ + 2H_2 \rightarrow n\text{-butyrate}^- + 2H_2O$	×1	−47.55	−44.10
		$2\ lactate^- + H^+ \rightarrow n\text{-butyrate}^- + 2CO_2 + 2H_2$	×2.5	−209.35	−232.55
				Total = −256.90	**Total =** −276.65
(j) Lactate reduction to propionate	*Selenomonas ruminantium*	$lactate^- + H_2O \rightarrow acetate^- + CO_2 + 2H_2$	×1	28.51	25.96
		$lactate^- + H_2 \rightarrow propionate^- + H_2O$	×2	−86.63	−85.21
				Total = −58.12	**Total =** −59.25

The directional feasibility of this metabolic reaction is dictated by the standard Gibbs free energy balance (ΔG°). For the reaction to be spontaneous and for the bacteria to derive the energy required for their maintenance and growth, the overall thermodynamic balance must be exergonic. The historical model using ethanol as an electron donor presents naturally favourable thermodynamics, which explains its frequent use in pioneering studies.

However, in the context of valorising raw industrial waste such as citrus or brewery residues, the primary fermentation is dominated by acetate and carbon dioxide, with a virtual absence of ethanol. In such an environment, the direct condensation of acetate molecules to form butyrate or caproate, without the intervention of a powerful external electron donor, is an endergonic reaction.

According to the bioenergetics of the carboxylate platform, trying to drive the direct reduction of acetate into butyrate using molecular hydrogen as a sole gaseous donor yields a standard Gibbs free energy change of only -7.22 kJ/mol at 37°C (Agler et al. 2011). Under real bioreactor conditions, such a weak thermodynamic driving force quickly leads to an endergonic state, creating a bioenergetics deadlock that halts further carbon chain elongation unless a continuous energetic influx is maintained.

The bacteria thus find themselves in a true bioenergetic deadlock: the rBOX reactions cannot be triggered spontaneously. The system is thermodynamically trapped at the SCCA stage. It is precisely this biophysical limitation that makes an intervention indispensable to artificially force the reaction by altering the thermodynamic equilibrium of the bioreactor.

2.2.3 Hydrogen as a power source

To overcome the thermodynamic deadlock inherent in mixed cultures lacking organic electron donors, one engineering strategy is to supplement the bioreactor with a powerful inorganic donor. Gaseous hydrogen (H_2) has emerged as a highly promising alternative today, particularly when coupled with carbon dioxide in the form of syngas or direct injection (Spirito et al. 2014). The effectiveness of hydrogen relies on its highly electronegative standard redox potential (E° = -414 mV at pH 7). This characteristic makes it an ideal electron carrier to push endergonic reduction reactions. Within the microbiome, H_2 drives rBOX through two main metabolic pathways. On one hand, it can be used directly by certain chain-elongating strains through complex electron bifurcation mechanisms. On the other hand, it fuels the guild of homoacetogenic bacteria, which convert the H_2/CO_2 couple into de *novo* acetate via the Wood-Ljungdahl pathway (Figure 6), thereby continuously supplying the system with the primers and organic donors required for the rBOX cycle (Spirito et al. 2014).

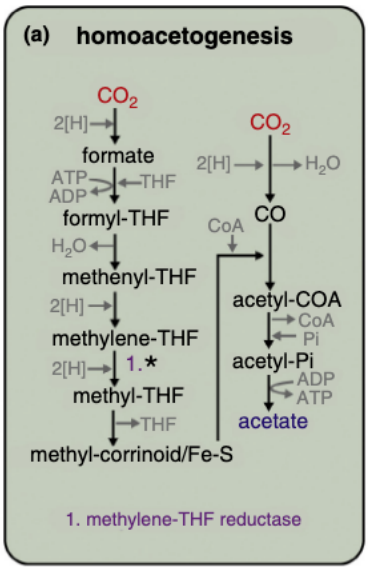

Figure 6. Homoacetogenesis (Spirito et al. 2014)

When organic substrates derived from complex residues are exhausted, this metabolic coupling transitions into a distinct secondary elongation phase solely driven by gaseous inputs. The biochemical signature of this process translates into a specific H_2/CO_2 molar consumption ratio of approximately 3 (Figure 7) (Henry et al. 2023a).

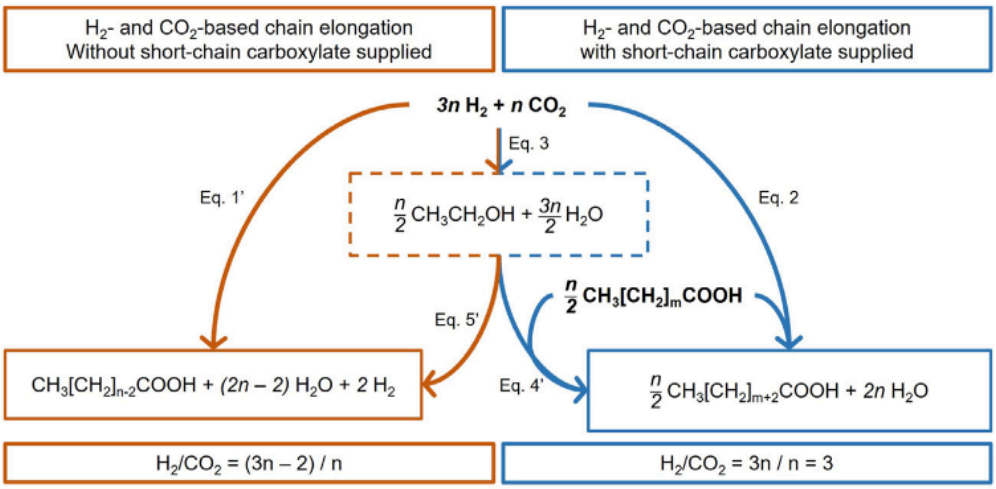

Figure 7. Stoichiometric balances of the H2 and CO2 conversion that can lead to MCCA (Henry et al. 2023a)

Thermodynamically, this pathway is highly exergonic, operating at a stable standard Gibbs free energy change of -143.9 ± 0.6 kJ/mol of produced carboxylate, regardless of the initial precursor chain length (m). This specific stoichiometry and favourable bioenergetics confirm that accumulated SCCAs can be systematically condensed into medium-chain architectures through the direct consumption of inorganic H_2 and CO_2 (Henry et al. 2023a).

However, implementing this gas-driven strategy involves bioprocess engineering challenges, primarily related to gas-liquid mass transfer. Because hydrogen is a poorly water-soluble molecule, it is imperative to maintain a high partial pressure in the bioreactor's headspace and to optimize agitation to maximize its bioavailability for the suspended microorganisms.

Nevertheless, while the supply of H_2 lifts the thermodynamic barrier for chain elongation, it simultaneously introduces a major vulnerability into the system. In a non-sterile, open mixed culture, hydrogen is the preferred substrate for another highly competitive and resilient microbial guild: hydrogenotrophic methanogenic Archaea. Without a rigorous control strategy, the energy injected for elongation is rapidly short-circuited toward methane production, thereby ruining the objective of the carboxylate platform. This competitive diversion is clearly illustrated during mixed culture fermentations under a H_2/CO_2 atmosphere, where an accidental shift to a methanogenic phase can lead to a doubling of gas consumption completely misrouted toward methane synthesis, which abruptly halts any ongoing short-chain carboxylate elongation (Henry et al. 2023a).

2.3 The challenge of mixed cultures

2.3.1 Benefits of mixed cultures

In the field of industrial biotechnology, using pure microbial cultures for metabolite production requires expensive infrastructure. Maintaining strict sterility and using synthetic or highly refined substrates generate operational and energy costs that hinder the economic viability of the process, particularly for waste valorisation. Conversely, microbiome engineering relies on the use of open mixed cultures. This biotechnological approach leverages complex, non-sterile microbial consortia capable of self-assembling and adapting to the environmental conditions imposed by the bioreactor (Kleerebezem and van Loosdrecht 2007).

The primary advantage of these mixed cultures lies in their extraordinary robustness and their ability to process raw and heterogeneous substrates, such as agro-industrial residues. Within this microbiome, multiple bacterial guilds coexist in syntropy. Hydrolytic and acidogenic bacteria break down complex polymers to continuously provide the metabolic precursors that will then be used by the chain-elongation guild (Spirito et al. 2014).

While historical elongation system fuelled by reduced soluble co-substrates (such as ethanol or lactate) allow hydrolysis, acidogenesis, and chain elongation to operate synergistically in a single stage, valorising carbohydrate-rich residues that lack these reduced electron donors requires engineered multi-phase configurations. In such setups, primary biomass acidogenesis is sequentially coupled with external gaseous hydrogen supplementation—typically delivered within a H_2/CO_2 headspace atmosphere—to supply the necessary electron driving force for the chain elongation stage (Henry et al. 2023b).

2.3.2 The thermodynamic short-circuit: methanogenic competition

However, the primary challenge inherent in open mixed cultures is the difficulty of selectively directing metabolic fluxes towards the desired product. In a non-sterile ecosystem, the supply of an electron donor as energetic and diffusible as gaseous hydrogen stimulates not only rBOX but also awakens all microorganisms capable of oxidizing it. In particular, hydrogen serves as an excellent substrate for the development of highly resilient hydrogenotrophic methanogens,

whose sudden activation can aggressively outcompete the chain-elongation guild by diverting the available electron flux towards methane synthesis (Henry et al. 2023a).

Among these competitors, hydrogenotrophic methanogenic Archaea pose the most critical threat to the carboxylate platform. These microorganisms, ubiquitous in anaerobic environments, possess an affinity and a growth rate on hydrogen that frequently exceed those of homoacetogenic and chain-elongating bacteria (González-Cabaleiro et al. 2013).

Stoichiometrically, these archaea catalyse the reduction of carbon dioxide by hydrogen to form methane : $CO_2 + 4H_2 \rightarrow CH_4 + 2H_2O$ Thermodynamically, methanogenesis is the most favorable terminal pathway in these ecosystems compared to competing pathways such as homoacetogenesis (González-Cabaleiro et al. 2013). Consequently, without an artificial selective pressure, methanogens inevitably end up dominating the microbiome. They act as a powerful « electron vacuum », short-circuiting the electron flux supplied via gaseous hydrogen and bringing carbon chain elongation to a complete halt (Agler et al. 2011). Maintaining the elongation window therefore requires the deployment of targeted inhibition strategies to specifically repress the methanogenic guild while preserving rBOX activity.

2.4 Methanogenesis inhibition and the role of the substrate

2.4.1 Conventional inhibitors vs natural inhibitors

To counteract the thermodynamic short-circuit induced by methanogens, various inhibition strategies have been developed in bioprocess engineering. The most classic approach relies on the addition of synthetic chemical inhibitors, the most documented being 2-bromoethanesulfonic acid (BESA). BESA is a structural analogue of coenzyme M, which is essential for methanogenesis, and acts as a highly potent competitive inhibitor (Steinbusch et al. 2011). However, the use of such compounds on an industrial scale is economically unrealistic and ecologically unsound, as BESA is an expensive and toxic chemical that contaminates the final digestate.

Other physical approaches, such as heat shocks or operating at very acidic pH (<5.5), are also employed. Although they can inactivate methanogens which are often sensitive to extreme fluctuations, these methods are highly energy-intensive or risk simultaneously inhibiting the

guild of chain-elongating bacteria, thereby reducing the overall yields of the bioprocess (Stamatopoulou et al. 2020).

Faced with these limitations, an emerging and much more interesting strategy involves exploiting the intrinsic toxicity of certain co-substrates. The objective is to use organic waste that naturally contains selective antimicrobial compounds, thus transforming the carbonaceous substrate into a microbiome control tool (Nzeteu et al. 2018).

2.4.2 The potential of essential oils: the example of D-limonene

Residues from the citrus industry (orange and lemon peels) constitute a substrate of choice for this approach. Besides their richness in soluble carbohydrates (such as pectin), which provide the carbon required for acidogenesis, this waste contains significant amounts of essential oils, composed of more than 90% D-limonene. D-limonene (Figure 8) is a cyclic monoterpene known for its strong antimicrobial properties, and particularly for its acute toxicity towards methanogenic archaea (B. Ruiz and Flotats 2014).

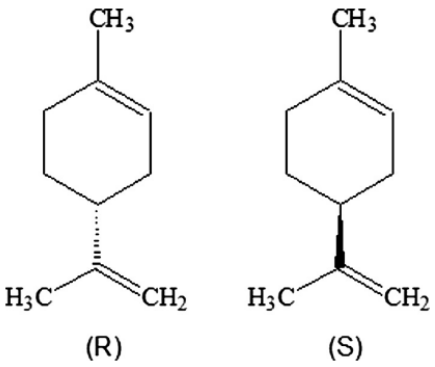

Figure 8. Structural formula of limonene

The mechanism of action of D-limonene is based on its highly hydrophobic nature. It inserts itself into the lipid bilayer of the microorganisms' cell membrane, causing a loss of structural integrity. This membrane disruption leads to an increase in permeability, leakage of intracellular ions and ultimately the dissipation of the proton motive force (PMF) essential for ATP synthesis and cell survival (Figure 9) (Carneiro et al. 2020). Methanogenic archaea, due to the specific composition of their membrane (consisting of ether-linked isoprenoid lipids),

prove to be particularly vulnerable to this steric perturbation compared to fermentative bacteria (Sikkema et al. 1995).

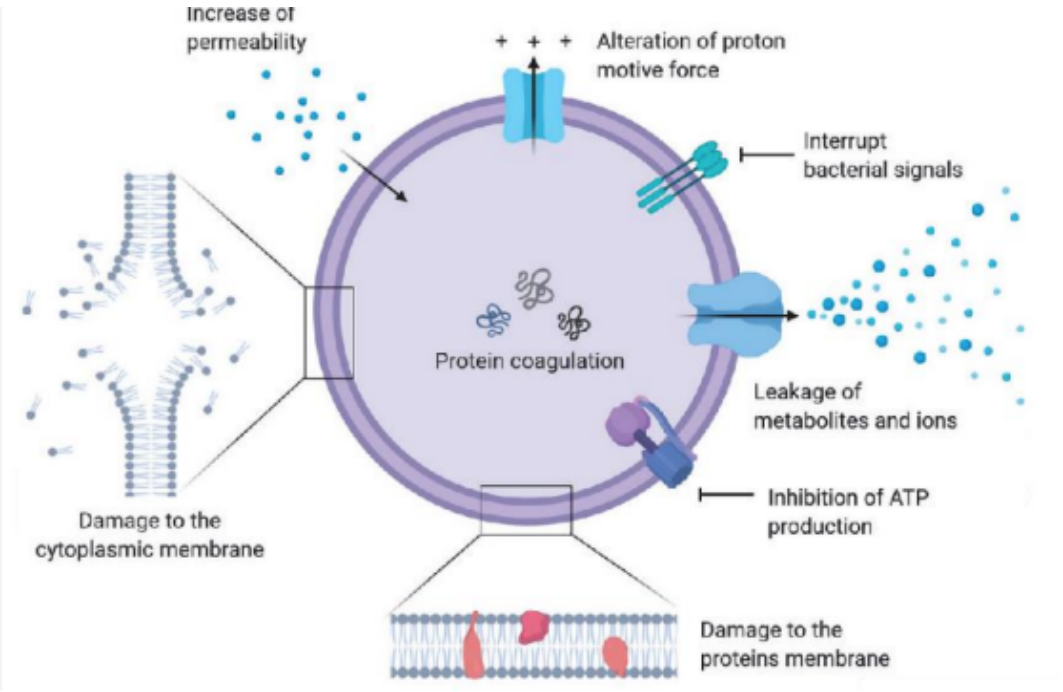

Figure 9. General antibacterial mechanisms of essential oils (Carneiro et al. 2020)

Consequently, the release of D-limonene during substrate degradation exerts a marked, temporary inhibitory effect on methanogenic archaea. Specifically, D-limonene disrupts microbial cell membranes and preferentially suppresses hydrogenotrophic methanogenesis, resulting in a transient accumulation of SCCAs and molecular hydrogen. However, as demonstrated by Ruiz and Flotats (2016), this methanogenic suppression is inherently reversible. D-limonene undergoes anaerobic biotransformation into secondary compounds (such as α-terpineol and cymene), allowing for microbial adaptation and the progressive recovery of methanogenic activity over time. Consequently, while D-limonene naturally induces a temporary arrest of methanogenesis, maintaining long-term inhibition in continuous processes requires additional operational controls to counteract microbial adaptation and inhibitor clearance (Begoña Ruiz and Flotats 2016).

2.5 Nutritional balance and co-digestion

2.5.1 The importance of bioavailable nitrogen and the C/N ratio

While the inhibition of methanogenesis is a *sine qua non* condition for the accumulation of carboxylic acids, it is not sufficient to guarantee a high-performing bioprocess. The microbiome requires a balanced nutritional environment to ensure cellular maintenance and the synthesis of the enzymatic machinery, particularly the enzymes catalysing rBOX. In this regard, the carbon/nitrogen (C/N) ratio of the feedstock is a critical parameter governing microbial growth and metabolic distribution (Liu et al. 2025).

In mixed-culture anaerobic systems, the impact of the C/N ratio is tied to electron efficiency, defined as the percentage of electron equivalents transferred from consumed substrates into the target products. In batch fermentations utilizing ethanol and butanoic acid, evaluating discrete C/N ratios demonstrated that an intermediate range between 3 and 25 maintains a strongly reducing environment favourable to carbon chain elongation. Within this window, electron efficiency toward caproic acid reached up to 72.9% (at C/N = 3), while preventing the metabolic blockages observed at extreme values. Empirical evaluation revealed that a C/N ratio of 3 yielded the highest caproic acid concentration (6175.9 mg/L), whereas a ratio of 15 further improved process purity by reducing acetate selectivity down to 3.4% (Liu et al. 2025).

Conversely, over-supplementation of nitrogen must be carefully avoided. An excessively low C/N ratio under high initial carbon loads requires massive ammonium addition, leading to severe chemical toxicity. For instance, at a C/N ratio of 1 with 120 mmol/L ethanol and 60 mmol/L butanoate, the total ammonium (NH_4^+) concentration reaches 7.2 g/L. High ammonium densities (> 2-5 g/L) induce severe cellular stress, which literature associates with potential intracellular reactive oxygen species (ROS) generation, membrane damage, and a decline in the cytoplasm NADH/NAD+ redox pair availability. This metabolic disruption impairs key rBOX enzymes and promotes excessive ethanol oxidation (EEO) to acetate (2444 mg/L), alongside the accumulation of unextended butanoate (4807 mg/L). Under these hyper-ammoniacal conditions, the overall electron efficiency of the system collapses to 36.6%, causing the final caproic acid concentration (1910.5 mg/L) to drop to only 31% of the performance achieved at C/N = 3 (Liu et al. 2025).

On the other hand, when the substrate exhibits an excessively high C/N ratio (>58), the resulting nitrogen deficiency severely impairs microbial growth and synthesis rates. Within the context of chain elongation, a lack of bioavailable nitrogen hinders the enzymatic expression

of the chain-elongating guild, leading to incomplete substrate conversion and the accumulation of intermediates. For instance, shifting the C/N ratio upwards to extreme values of 58, 75 or 100 leads to a significant decrease in caproic acid production by 26.2%, 35.4%, and 39.4%, respectively, as electron transfer becomes blocked by the accumulation of unextended butanoic acid (Liu et al. 2025).

Orange peels, although an excellent supplier of rapidly biodegradable carbon, presents a highly unbalanced nutritional profile. Its C/N ratio is generally too high (>40 :1), reflecting a severe nitrogen deficiency, with values specifically characterized at 43.76 for raw orange pulp (Atelge 2021). Nitrogen, however, is the fundamental building block for amino acids, proteins and nucleic acids. In a mixed culture system, such a deficiency drastically limits the specific growth rate of acidogenic and chain-elongating bacteria. Metabolism is thus hindered, not by a lack of energy or electrons, but by a strict anabolic limitation that disrupts the enzymatic machinery necessary to sustain the rBOX cycle.

2.5.2 Valorisation of malting byproducts in co-digestion

To overcome this nutritional deficiency without resorting to the addition of expensive synthetic ammonium salts, bioprocess engineering favours the co-digestion strategy. This approach involves mixing the main carbonaceous substrate with a co-substrate rich in bioavailable organic nitrogen. In this study, residues from the malting industry—specifically rootlets and green malt—were selected as co-substrates to evaluate this potential synergy.

Rootlets constitute a major byproduct generated during the kilning and cleaning stages of the malting process. Biochemically, these residues are characterized by a high protein content alongside accessible carbohydrates and essential minerals. During anaerobic digestion, the enzymatic hydrolysis of malting proteins is expected to gradually release peptides and free amino acids into the fermentation broth. This progressive breakdown provides a continuous source of organic nitrogen, which can support sustained bacterial growth while reducing the risk of sudden ammonia toxicity.

Within the context of the carboxylate platform, the co-digestion of orange peels and malting byproducts is hypothesized to yield a balanced, self-sustaining fermentation medium. In this

proposed framework, orange peels serve as the primary source of easily fermentable carbohydrates and antimicrobial selection agents, whereas malting residues are intended to restore stoichiometric balance by supplying organic nitrogen and micronutrients required for microbiome robustness.

2.6 Synthesis of literature knowledge and research objectives

The review of the scientific literature highlights the potential of the carboxylate platform to valorise residual biomass into high-value molecules, such as caproic acid. Although H_2 gas injection thermodynamically supports chain elongation, maintaining this bioprocess in open mixed cultures is systematically challenged by electron competition from methanogenic archaea.

Because conventional chemical inhibitors present economic and environmental drawbacks, relying on the endogenous selective toxicity of specific feedstocks—such as the D-limonene present in orange peels—represents an alternative concept worthy of exploration. However, the mono-digestion of citrus waste is constrained by an unbalanced C/N ratio, which limits microbial growth. While co-digestion with organic nitrogen sources, such as malting byproducts (rootlets and green malt), is expected to address this nutritional imbalance, the combined effects of these substrates remain to be fully characterized.

Specifically, the temporal dynamics of this multi-substrate system within open microbiomes—particularly regarding the duration of the "elongation window" before methanogenic recovery—remain poorly documented. Therefore, the objective of this work is to investigate the interplay between D-limonene toxicity, C/N balancing through malting byproducts, and H_2 supplementation to evaluate the feasibility and boundaries of sustained caproic acid production.

3 Objectives

The primary aim of this thesis is to evaluate and optimize the anaerobic fermentation of orange peel waste for carboxylate production using sewage sludge from a wastewater treatment plant, with a specific focus on steering metabolic fluxes toward high-value medium-chain carboxylic acids (MCCAs). To achieve this goal, the research is structured around four specific objectives.

The first objective focuses on assessing the anaerobic biodegradability of orange peel waste under controlled, neutral pH conditions. This phase aims to evaluate the degradation kinetics of orange peels and identify potential inhibitory phenomena related to essential oils (specifically D-limonene) across different fermentation media.

The second objective investigates the influence of headspace composition on electron allocation. By comparing an exogenous CO_2/H_2 supply against an inert nitrogen atmosphere, this work aims to elucidate the competition and synergy between homoacetogenesis and microbial chain elongation via reverse β-oxidation (rBOX), determining how gaseous electron donors alter the final short-chain carboxylic acid (SCCA) spectrum and product distribution.

To counteract the nutritional constraints of orange peels, the third objective compares the supplementation of green malt versus rootlets. This comparative analysis aims to identify the most effective co-substrate for supplying bioavailable organic nitrogen and essential growth factors to sewage sludge, evaluating their respective impacts on carboxylate production kinetics and overall acid yields.

The final objective centres on analysing the distribution profiles of fermentative metabolites across all tested configurations. Through this comprehensive profiling, this study seeks to define the operational conditions that successfully steer electron fluxes toward higher-value molecules, particularly medium-chain carboxylic acids (MCCAs).

4 Material and method

4.1 Substrates and inoculum

4.1.1 Substrates origin and preparation

Orange peel waste, serving as the primary carbon source, was obtained fresh from a local commercial contributor (Carrefour, Ottignies-Louvain-la-Neuve, Belgium). The peels were manually chopped into fragments (=2 cm2) and homogenized into a fine fibrous pulp using a high-performance knife mill (IKA MultiDrive basic, IKA-Werke GmbH & Co. KG, Germany). The milled pulp was stored in sealed airtight containers at -20°C to prevent premature biochemical degradation and thawed prior to reactor inoculation.

Two industrial malting by-products—rootlets (malt culms) and green malt (germinated barley prior to kilning)—were supplied by Boormalt (Antwerp, Belgium) to serve as organic nitrogen and micronutrients sources. The residues were milled without chemical pretreatment and stored at -20°C.

4.1.2 Inoculum

Raw municipal return activated sludge (RAS) was collected from the municipal wastewater treatment plant of Mont-Saint-Guilbert, Belgium. The sludge was collected fresh from the secondary settling return line, homogenized by gentle stirring, and introduced into the reactors without thermal, chemical, or physical pretreatment, thereby providing a native, fully viable microbiome.

4.2 Experimental setup and reactor operation

4.2.1 Bioreactor design

Batch fermentations were performed in parallel using 12 customized bench-scale glass bioreactors operated in biological triplicate (n = 3). Each reactor consisted of a 2.3 L borosilicate glass bottle (Schott Duran, Germany, calibrated total internal volume: 2305 ± 15 mL).

Airtight sealing was provided by a pierced GL45 screw cap compressing a stainless-steel headpiece against a fluoroelastomer O-ring gasket. The headpiece featured two dedicated ports:

Gas port: Equipped with an internal flexible PVC tube fitted with a two-way Luer-Lock valve for headspace flushing, gas pressure measurement, and biogas sampling.

Liquid port: Connected to an internal flexible dip tube extending to the bottom of the vessel (bevelled at its lower tip to prevent fibrous particle clogging) and sealed externally with a Mohr pinchcock valve for liquid sampling and reagent addition.

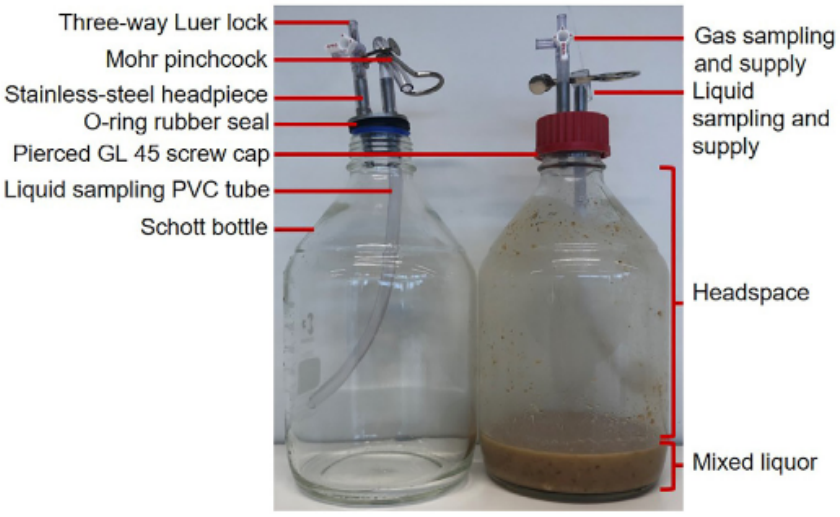

Figure 10. Assembled and filled bioreactors (Henry et al. 2023a)

4.2.2 Bioreactor start-up and initial pressurization

Each reactor was loaded with 34 g of mixed liquor slurry comprising orange peel pulp (15.4 g COD), malting co-substrate (0.6 — 0.7 g COD), and raw municipal activated sludge (0.1 g COD).

After hermetic sealing, the headspaces were flushed for 10 minutes with their designated gas mixture (N_2 or H_2/CO_2) at a flow rate of 4 L/min to evacuate residual oxygen. The absolute headspace pressure was adjusted to 1.3 ± 0.02 bar using a digital piezoresistive pressure transmitter (UNIK 5000, Balker Hughes Druck, Germany). The reactors were placed horizontally on an orbital shaker (Lab-Shaker, Kühner, Switzerland) operating at 120 rpm inside a temperature-controlled incubator maintaining at 37 ± 0.5°C.

4.2.3 Experimental matrix

Table 3. Summary of initial experimental configurations in the batch bioreactors (n = 3).

Condition	Primary Substrate	Inoculum	Co-substrate	Headspace Atmosphere	Operating Total Pressure
1	Orange peel	Return activated sludge	Rootlets	N_2 (100%)	1.3 ± 0.02 bar
2	Orange peel	Return activated sludge	Green malt	N_2 (100%)	1.3 ± 0.02 bar
3	Orange peel	Return activated sludge	Rootlets	H_2/CO_2 (77/23%)	1.3 ± 0.02 bar
4	Orange peel	Return activated sludge	Green malt	H_2/CO_2 (77/23%)	1.3 ± 0.02 bar

4.3 Monitoring and sampling protocol

Monitoring and liquid-gas sampling were carried out thrice weekly (Monday, Wednesday, Friday) according to the following sequential protocol:

1. Initial bioreactor mass and headspace pressure: The initial total mass of each bioreactor was recorded to track mass balance evolution and cumulative liquid removal over time. The total absolute headspace pressure in each reactor was recorded with the digital UNIK 5000 pressure transmitter connected to the gas Luer-Lock valve.

2. Biogas sampling: A 20 mL gas sample was collected into a gas-tight polypropylene syringe (BD Plastipak, USA) equipped with a three-way stopcock valve and immediately transferred to the gas chromatograph for composition analysis.
3. Post-sampling pressure: Headspace pressure was recorded immediately following gas sampling to account for mass withdrawal.
4. Mixed liquor sampling: A liquid sample was collected through the dip tube using a tared 50 mL polypropylene syringe. The syringe containing the ML was weighed to calculate the withdrawn sample mass by tare subtraction. The mass of mixed liquor remaining in the bioreactor was determined by weight difference.
5. pH measurement and micro-titration: A 2 mL sub-aliquot of the withdrawn ML was transferred into a glass tube. The pH was measured with a calibrated glass electrode (TWT SenTix 41). The aliquot was titrated with 2 M KOH to determine the specific proton production.
6. Phase separation and storage: The remaining sampled ML was transferred into tared 15 mL Faclon tubes and centrifuged (Heraeus Megafuge 40, Thermo Scientific). Clarified supernatant and wet solid pellets were separated, weighed, and stored a -20°C for subsequent soluble COD, carboxylate extraction and solid TS/VS determinations.
7. pH neutralization and volume maintenance: Based on the titration results and the exact mass of ML taken, the required volume solution of 2 M KOH with water was injected into the reactors to restore the pH to 7.
8. Headspace atmosphere management:
    - Inert conditions: Headspaces pressure were adjusted with pure N_2 to reach 20 mbar above the operating setpoint (1.32 bar absolute).
    - Reducing conditions: Headspaces were flushed for 2 min at 4 L/min with the certified H_2/CO_2 mixture to restore the initial H_2/CO_2 molar ratio and prevent CO_2 progressive depletion, before pressurizing to 1.32 bar absolute.
9. Final state verification: A second 20 mL gas sample was analysed to record the post-monitoring headspace composition and confirm the absence of residual O_2. The final headspace pressure and the final total bioreactor mass were recorded.

4.3.1 Re-inoculation procedure (Day 20)

A re-inoculation was conducted on Day 20 across all 12 bioreactors. Immediately following inoculation, reactor headspaces were flushed for 5 minutes with their assigned gas phase and repressurized to 1.3 bar.

4.3.2 End of the incubation and sample portioning (Day 64)

At the end of the 64-days cultivation period, the final headspace pressure and gas composition were recorded. Bioreactors were opened, and the total slurry was weighed and centrifuged in tared centrifuge buckets.

The clarified supernatant and solid pellet fractions were separated and analysed gravimetrically for total solids (TS), volatile solids (VS), and chemical oxygen demand (COD).

4.4 Analytical methods

4.4.1 Gravimetric determination

Total solids (TS), volatile solids (VS), and mineral ash content were determined gravimetrically in triplicate on both liquid and solid fractions in accordance with standard methods 2540 G (APHA, 1998). Clean porcelain crucibles were pre-calcined in a muffle furnace at 550°C for 2 hours, cooled to room temperature in a glass desiccator containing silica gel, and tared on an analytical balance to record the tare mass (m_0). A representative aliquot of fresh sample was transferred into the crucible and weighed immediately to determine fresh sample mass ($m_{fresh} = m_1 – m_0$).

Crucibles were then placed in a drying oven at 105°C for 24 hours to evaporate free and moisture water. After cooling in a desiccator, the dry mass was recorded ($m_{dry} = m_2 – m_0$) to calculate TS:

$$TS = \frac{m_2 - m_0}{m_1 - m_0} \quad (g\ TS/g\ FW)$$

The dried residues were subsequently calcined in a muffle furnace at 550°C for 4 hours to combust all volatile organic matter. Following desiccation, the final mass of the mineral residue (m_3) was recorded to determine ash content and VS:

$$Ash = \frac{m_3 - m_1}{m_1 - m_0} \quad (g\ Ash/g\ FW)$$

$$VS = \frac{m_2 - m_3}{m_1 - m_0} \quad (g\ VS/g\ FW) \ \ or \ \ VS_{TS} = \frac{m_2 - m_3}{m_2 - m_0} \quad (g\ VS/g\ TS)$$

4.4.2 Chemical oxygen demand quantification

Soluble COD was determined on clarified supernatants following centrifugation (10 000 x g, 5 min) using closed reflux colorimetric dichromate digestion kit (Spectroquant kit 1.14555.0001, measuring range 500 — 10 000 mg COD/L, Merck KGaA, Germany). A 1 mL volume of appropriately diluted sample was mixed with 1 mL of demineralized water in the reaction cell, mixed and digested for 2 hours at 148°C in a preheated thermoreactor (Spectroquant TR 620 Merck KGaA). After cooling to room temperature in a light-protected rack, green Cr^{3+} absorbance was quantified at λ = 605 nm using a spectrophotometer (Spectroquant Pharo 300, Merck KGaA) calibrated with internal factory curves.

Total solid-liquid COD was quantified by open reflux digestion in accordance with Standard Method 5220 B (APHA, 1998). A known mass of homogenized slurry (containing approximately 30 mg VS) was digested in a 500 mL round-bottom flask with 50 mL of standardized 0.25 N $K_2Cr_2O_7$, 0.4 g $HgSO_4$ (to complex chloride interferences), and 66 mL of silver sulfate catalyst dissolved in concentrated sulfuric acid (6.6 g Ag_2SO_4/L H_2SO_4). The mixture was refluxed under a Liebig condenser for 30 minutes. After cooling and rinsing the condenser with 180 mL of

demineralized water, unreacted dichromate was titrated against standardized 0.25 N ferrous ammonium sulfate using ferroin as redox indicator.

4.4.3 Biogas composition analysis

Headspace gas composition was measured by gas chromatrography coupled to thermal conductivity detectors (CompactGC 3.0, Global Analyser Solutions, Interscience, The Netherlands). The analyser incorporates two parallel chromatographic channels operated isothermally:

Front channel (CO_2 and H_2O): Fitted with a Rt-QBond non-polar porous polymer capillary column (10 m x 0.32 mm, Restek, France) maintained at 60°C. Helium was used as carrier gas at a constant flow rate of 1 mL/min and a head pressure of 80 kPa.

Back channel (H_2, O_2, N_2, CH_4): Configured with a Rt-QBond pre-column (2 m x 0.32 mm) connected via an automated, timed three-way backflush switching valve to a Molsieve 5A capillary column (7 m x 0.32 mm, Restek, France) maintaining at 70°C. Argon was used as carrier gas at 1 mL/min and 70 kPa to ensure high detection sensitivity for hydrogen. The switching valve backflushed CO_2 and moisture out of the pre-column before they could reach and contaminate the molecular sieve.

TCD detector blocks were heated to 90°C and tungsten-rhenium filaments were maintained at 170°C. Gas samples were manually injected through a 25 µL fixed injection loop. Compound identification and integration were performed using Chromeleon 7 software (Thermo Fisher Scientific, USA). The instrument was calibrated with five certified multi-component standard gas mixtures (Air Liquide, France), yielding a detection limit of 0.1% v/v.

4.4.4 Soluble metabolic extraction and chromatographic quantification

Volatile fatty acids (VFAs), carboxylates and alcohols were extracted by liquid-liquid extraction into diethyl ether prior to gas chromatography analysis:

1. Extraction protocol: In glass screw-top Pyrex test tubes, 0.5 mL of centrifuged supernatant (or calibration standard solution) was mixed with 1.5 mL of demineralized water and approximately 1 g of NaCl to promote phase separation via salting-out.

2. Internal standardization: A volume of 0.2 mL of 4-methylvalerate (4-MV, 1 g/L aqueous stock solution) was added as internal standard.

3. Acidification and solvent extraction: Samples were acidified with 1 mL of 2 M H_2SO_4 to convert all carboxylates into their uncharged protonated forms, immediately followed by 2 mL of pure diethyl ether (Sigma-Aldrich). Tubes were sealed with PTFE-lined screw caps, shaken vigorously by hand for 1 minute, and centrifuged at 3 000 rpm for 1 minute to ensure clean phase boundary solution.

4. Sample recovery: The organic upper ether layer was recovered using a positive displacement micropipette and transferred into 1.5 mL glass GC vials sealed with airtight PTFE/silicone screw caps (VWR International, Belgium) to limit solvent evaporation during autosampler queuing.

4.4.5 Chromatographic separation

Ether extracts were analysed using a Trace GC gas chromatograph (Thermo Fisher Scientific, USA) equipped with an automated liquid sampler and a flame ionization detector (FID) maintained at 260°C. The column used was a DB-WAX Ultra Inert polar capillary column (30 m x 0.25 mm internal diameter, 0.25 μm film thickness, Agilent Technologies, USA). The injection was in split mode (1:10, split flow 12 mL/min) at an injector temperature of 250°C, using high-

purity N_2 as carrier gas at a constant column flow of 1.2 mL/min. The initial temperature held at 40°C for 1 minute and increased at a rate of 10°C/min for 20 minutes to 240°C and held this temperature for 22 minutes.

4.4.6 Quantification and calibration matrix

Peak detection, baseline integration, and calibration regressions were performed in Chromeleon 7. For each target analyte, peak areas were normalized against the 4-MV internal standard peak area to correct for volumetric variations during extraction and injection.

Calibration lines were constructed from two independent stock solutions (A & B) with alternative compound concentration levels. Each stock solution was serially diluted across three dilution levels, yielding a 9-point linear calibration curve forced through the origin (0;0).

4.4.7 Genomic DNA extraction

Genomic DNA was extracted using the ZymoBIOMICS™ DNA Miniprep Kit according to the manufacturer's instructions. Approximately 200 mg of samples were transferred into ZR BashingBead™ Lysis Tubes (0.1 & 0.5 mm) containing 750 µl of ZymoBIOMICS™ Lysis Solution. Mechanical lysis was performed using a bead beating device (max agitation for 25 min). Following homogenization, the tubes were centrifuged at 10 000 x g for 1 minute. To remove cellular and environmental debris, up to 400 µl of the supernatant was filtered through a Zymo-Spin™ III-F Filter by centrifugation at 8 000 x g for 1 minute. For DNA binding, 1 200 µl of ZymoBIOMICS™ DNA Binding Buffer was well mixed with the filtrate. 800 µL of the resulting mixture was loaded onto a Zymo-Spin™ IICR Column and centrifuging at 10 000 x g for 1 minute and discarding the flow-through each time. The column was subsequently washed with 400 µl of ZymoBIOMICS™ DNA Wash Buffer 1, followed by two successive washes with 700 µl and 200 µl of ZymoBIOMICS™ DNA Wash Buffer 2. Each wash step was followed by centrifugation at 10 000 x g for 1 minute.DNA elution was performed by adding 50 µL of ZymoBIOMICS™ DNase/RNase Free Water directly to the column matrix, incubating at room temperature for 1 minute, and centrifuging at 10 000 x g for 1 minute. Finally, to remove potential PCR inhibitors,

the eluted DNA was passed through a Zymo-Spin™ III-HRC Filter—previously prepared with 600 µl of ZymoBIOMICS™ HRC Prep Solution and centrifuged at 8 000 x g for 3 minutes —by centrifugation at 16 000 x g for 3 minutes. The purified DNA was then stored in a freezer at -20°C for downstream applications.

4.5 Calculation, conversion and mass balances

4.5.1 Headspace gas calculations and molar balances

The partial pressure of each gaseous species i (P_i) in the headspace at a given monitoring time t was calculated from the measured total absolute pressure (P_{tot}) and the dry volumetric/molar fraction (y_i) determined by GC-TCD:

$$P_i = P_{tot} \cdot y_i$$

The molar quantity of gas i (n_i) present in the reactor headspace was calculated using the ideal gas law:

$$n_i = \frac{P_{tot} \cdot y_i \cdot V_{headspace}}{R \cdot T}$$

4.5.2 Theorical chemical oxygen demand

The theorical COD represents the stoichiometric mass of oxygen required to fully oxidize an organic compound into CO_2 and H_2O. For a generic compound $C_xH_yO_z$, complete oxidation follows the stoichiometric reaction:

$$C_xH_yO_z + \left(x + \frac{y}{4} - \frac{z}{2}\right) O_2 \rightarrow x\, CO_2 + \frac{y}{2} H_2O$$

Using the molecular weights of oxygen and the compound, the mass-specific theorical COD factor was calculated as:

$$COD_{th} = \frac{8 \,.\, (4x + y - 2z)}{12.011x + 1.008y + 16z}$$

4.5.3 Sampling mass removal and dilution tracking

At each intervention, withdrawing an aliquot of volume V_{sample} removed a discrete mass of COD from the vessel:

$$\Delta COD_{sampled} = V_{sample} \,.\, COD_t$$

The dilution factor (δ) resulting from sample withdrawal and subsequent reagent compensation is modelled as:

$$\delta = \frac{V_{ML} - V_{sample}}{V_{ML}}$$

5 Results

5.1 Substrate and inoculum composition

The initial gravimetric properties (Total Solids, Volatile Solids) and Chemical Oxygen Demand (COD) of the primary feedstock, co-substrates, and microbial inoculum are summarized in Table 4.

Table 4. Initial physicochemical properties and COD distribution of substrates, co-substrates, and inoculum (n = 3).

Sample	TS (g TS/g FW)	VS (g VS/g TS)	VS content (g VS/g FW)	COD (g COD/g FW)	COD (g COD/g T S)	Mean COD (g COD/g VS)
Orange peel	0.211	0.957	0.202	0.270	1.280	1.337
Return-active sludge	0.041	0.428	0.017	0.025	0.527	1.233
Rootlets	0.956	0.850	0.810	1.150	1.200	1.420
Green malt	0.574	0.950	0.550	0.760	1.320	1.380

Orange peel waste presented a dry matter content of 0.211 g TS/g FW with a high volatile solid purity of 0.957 g VS/g TS, yielding an organic load of 1.28 g COD/g TS.

Malting byproducts both exhibited high organic densities: rootlets had the highest dry matter fraction with 1.2 g COD/g TS, while green malt had a dry matter content of 0.574 g TS/g FW and 1.32 g COD/g TS.

Return-activated sludge (RAS) contained low solids and a volatile solid fraction of 0.428 g VS/g TS, corresponding to 0.527 g COD/g TS and an organic-specific COD of 1.233 g COD/g VS.

5.2 Fermentation evolution

5.2.1 pH dynamics

The temporal evolution of pH across the four experimental conditions is shown in Figure 11. Throughout the batch cultivation, the pH of all reactors was manually adjusted back to approximately 7 using 2 M KOH during each monitoring event. Consequently, the biological acidification of the medium is characterized by the frequency and depth of the downward spikes observed between consecutive sampling points.

During the first phase of the experiment (Days 0 to 10), a rapid decrease in pH was recorded in all conditions. The pH values dropped from the initial setpoint to minimum values ranging between 4.3 and 4.7 within the first 48 hours. This sharp decrease was consistently observed across all replicates.

Between Days 10 and 23, the frequency and amplitude of the pH drop diminished in all setups. Notably, in Condition 3 (Reductive atmosphere - Rootlets), the pH profile remained completely stable, showing a flat horizontal line at 6.8 from Day 15 until Day 23, without requiring any alkaline addition. In contrast, the other three conditions maintained minor pH fluctuations during this period.

Following the re-inoculation on Day 20, a resumption of acidification was observed in the reactors. In Condition 3, the pH began to drop again, oscillating between 6.5 and 6.8. In Condition 4 (Reductive atmosphere - Green Malt), a regular acidification pattern was established, with the pH consistently decreasing to approximately 6.2 before each neutralization event until Day 64.

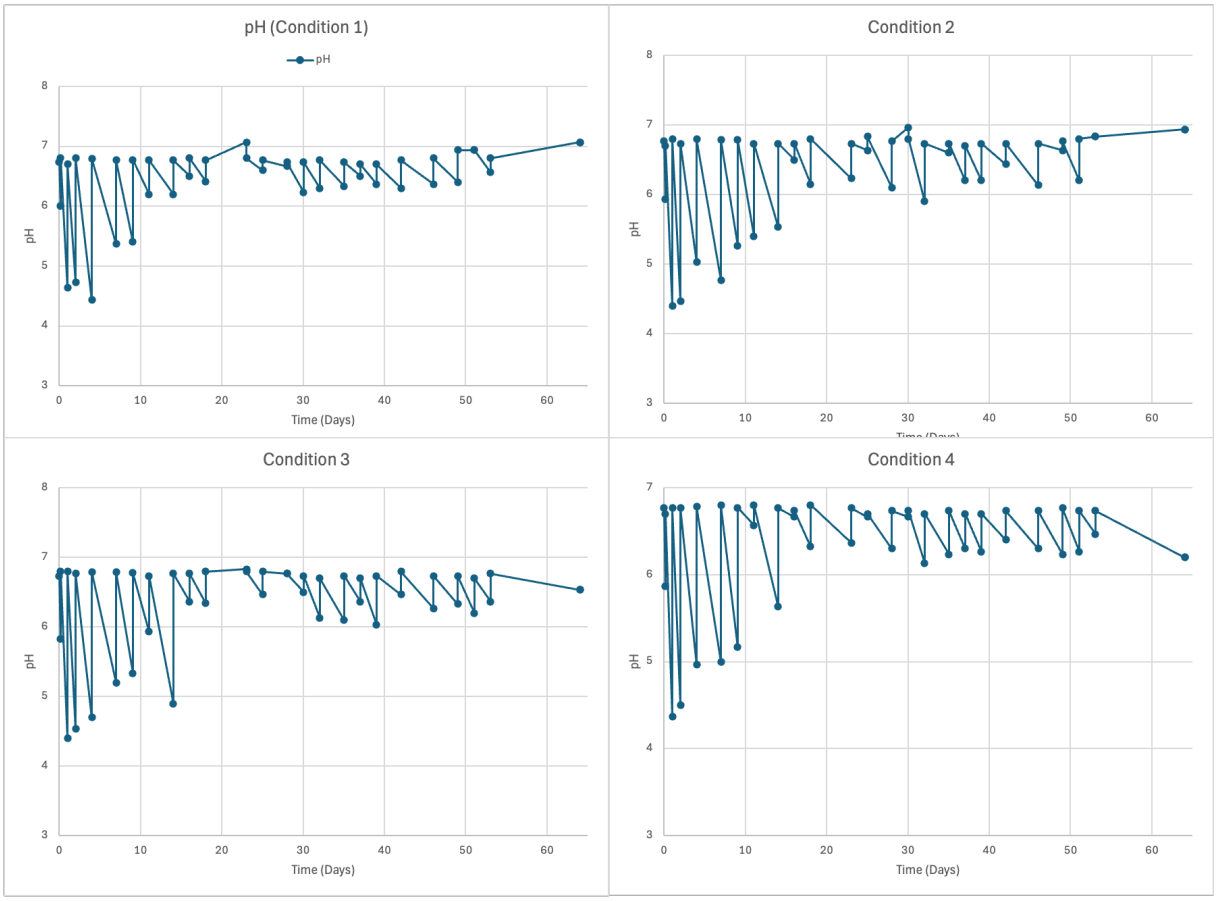

Figure 11. pH as a function of time across Conditions 1 to 4 (n = 3).

5.2.2 Headspaces gas composition

The headspace gas partial pressures (P_{H2}, PC_{O2}, P_{N2}, P_{CH4}, P_{O2}) and total pressure (P_{tot}) across the four conditions over the 64-day period are presented in Figure 12.

P_{O2} remained strictly at 0 bar under all conditions throughout the entire 64-days fermentation, confirming perfect gas tightness of the reactors and the maintenance of strict anaerobic conditions without atmospheric contamination.

N_2 atmosphere (Conditions 1 & 2): Maintained stable P_{tot} (1.2 — 1.45 bar) dominated by nitrogen (P_{N2} > 1.05 bar). Endogenous CO_2 release remained marginal ($P_{CO2} \leq 0.2$ bar), and both H_2 and CH_4 remained strictly undetected.

H_2/CO_2 atmosphere (Conditions 3 & 4): Exhibited intense gas dynamics with three distinct phases: a 24-day lag phase (P_{tot} = 1.35 — 1.45 bar), an active gas-consumption phase not long time after the re-inoculation at Day 20 (Days 25-42) with rapid H_2 drops to < 0.1 bar prior to flushes, and a methanogenic phase (Days 42-64) where CH_4 reached 0.28 — 0.3 bar.

Under N_2 (Condition 1 vs Condition 2): Both co-substrates displayed identical baseline profiles.

Under H2/CO2 (Conditions 3 vs 4): Both conditions overcame the latency period simultaneously following the Day 20 re-inoculation. Green malt displayed slightly faster gas consumption rates between Days 25 and 40 (steeper pressure drops), but both conditions transitioned to methanogenesis synchronously on Days 42-45 with identical final methane peaks (0.3 bar).

Figure 12. Headspace total and partial pressures over time across Conditions 1 to 4 (n = 3). Sawtooth profiles indicate biological gas consumption and intermediate re-pressurizations.

5.2.3 Gas consumption and production dynamics

The cumulative net consumption (+) and production (-) of gaseous species and the total gas balance in mol/m^3_r over the 64-day incubation period are shown in Figure 13 . The apparent cumulative accumulation of nitrogen observed across all reactors is an analytical calculation artifact stemming from successive liquid and gas samplings coupled with periodic re-pressurizations, rather than biological assimilation.

Under nitrogen headspace (Conditions 1 and 2), gas dynamics were characterized solely by acidogenic emissions without any methanogenic activity. Carbon dioxide was continuously released, reaching a cumulative production of -210 mol/m^3r in Condition 1 (Rootlets) and -180 mol/m^3r in Condition 2 (Green malt). Minor endogenous hydrogen production was also detected during the first 25 days before levelling off at -70 mol/m^3r for rootlets and -50 mol/m^3r for green malt. In both inert conditions, net methane generation remained strictly at 0 throughout the entire run.

Under reducing H_2/CO_2 atmosphere (Conditions 3 and 4), net cumulative gas exchanges remained negligible during the initial 20-day lag phase. Following the re-inoculation on Day 20, active gas consumption began on Day 24. Between Days 24 and 42, a steady and simultaneous uptake of hydrogen and carbon dioxide took place in the absence of methanogenesis, reaching +970 mol/m^3r of H_2 in Condition 3 and +914 mol/m^3r in Condition 4.

From Day 42 onward, a sharp metabolic transition occurred with the onset of methanogenesis, accumulating -450 mol/m^3r (Condition 3) and -475 mol/m^3r (Condition 4) of CH_4 by Day 64. This phase was accompanied by an acceleration in hydrogen uptake, culminating in total cumulative consumptions of +2470 mol/m^3r in Condition 3 and +2600 mol/m^3r in Condition 4, with final net CO_2 consumption reaching +440 and +510 mol/m^3r, respectively. Comparing the co-substrates, green malt supported higher cumulative acidogenic CO_2 release under N_2 and slightly higher overall H_2 and CO_2 consumptions under reducing conditions than rootlets, while following an identical kinetic pattern.

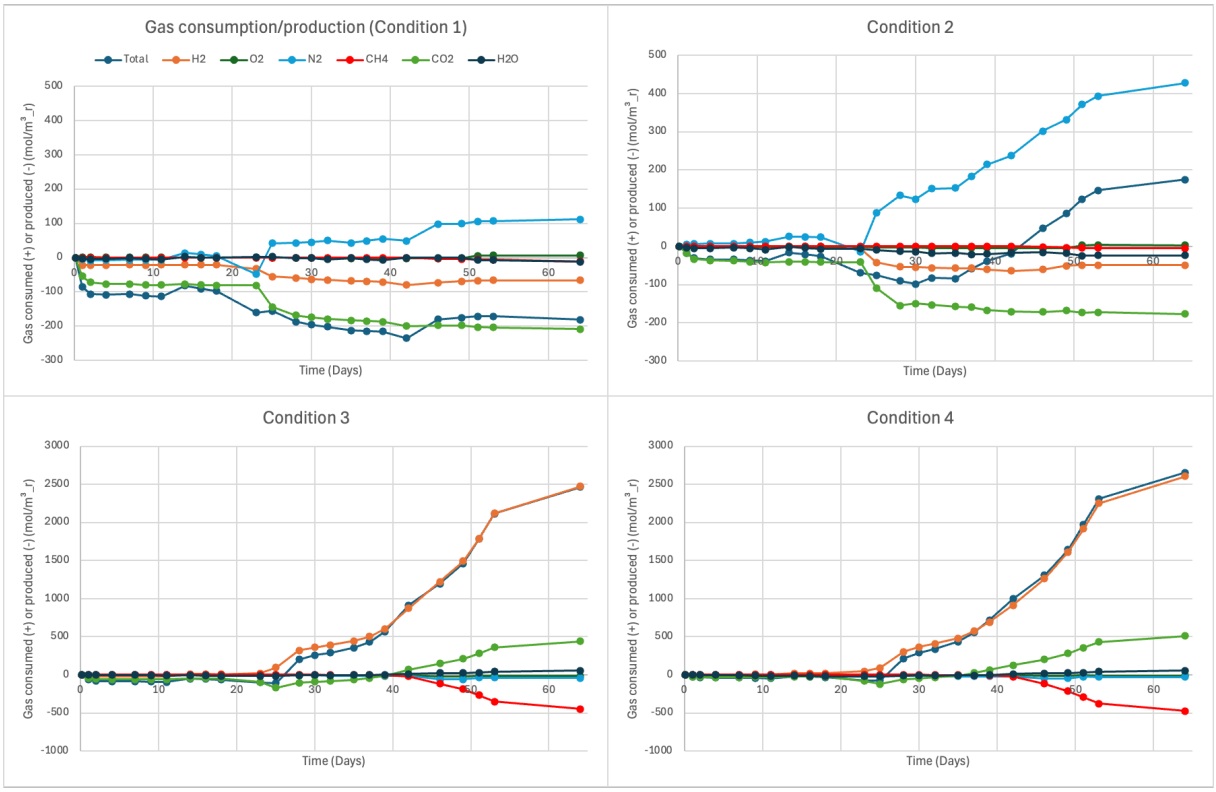

Figure 13. Cumulative net consumption (+) and production (-) of gaseous species and total gas balance across Conditions 1 to 4 (n = 3).

5.2.4 Metabolites concentrations

The evolution of individual soluble carboxylate concentrations (acetate C2, propionate C3, butyrate C4, valerate C5, caproate C6, and heptanoate C7) over the 64-day fermentation is shown in Figure 14.

During the initial 20-day latency period, carboxylate production remained inactive under all four conditions, with only residual concentrations of acetate present (1-2.4 g COD/L) and all other metabolites remaining below detection limits. Following the microbial re-inoculation on Day 20, soluble metabolite accumulation was triggered immediately across all reactors, with distinct product distributions determined by the headspace atmosphere.

Under nitrogen atmosphere (Conditions 1 and 2), fermentation was predominantly directed toward short-chain carboxylates. Acetate was the major metabolite throughout the run, rapidly rising to 9.5 g COD/L between Days 22 and 30 before stabilizing between 6 and 8 g

COD/L. Propionate peaked transiently at Day 22 (4-4.5 g COD/L) before slowly decreasing. Butyrate and valerate increased steadily to plateaus of 3.5-5 g COD/L. Chain elongation to medium-chain carboxylates was minor: caproate and heptanoate accumulated slowly after Day 25, reaching final values of 3.5-4.5 g COD/L and 2.1-2.7 g COD/L by Day 64. In Condition 1, the acute concentration spike observed on Day 46 represents an isolated analytical artifact, as concentrations returned to their expected baseline on Day 49.

Under reducing atmosphere (Conditions 3 and 4), the metabolic profile shifted toward elongated carboxylates. Valerate and butyrate became the dominant products. Following re-inoculation, C3 displayed a transient peak at Day 20 (5.6 g COD/L in Condition 3; 6.3 g COD/L in Condition 4) before being consumed down, coinciding with a rapid rise in C5 and C4. Maximum carboxylate accumulation occurred between Days 30 and 35, where C5 peaked at 11 g COD/L (Condition 3) and 12.8 g COD/L (Condition 4), while C4 peaked at 9.6 and 11.1 g COD/L, respectively. Caproate reached 6.7 g COD/L, while acetate remained lower. Between Days 37 and 42, coinciding with the methanogenic shift, a noticeable drop in all carboxylate concentrations occurred, stabilizing toward Day 64 at 7.7-10 g COD/L for C5, 8.2-8.6 g COD/L for C4, and 6-6.3 g COD/L for C6.

Comparing co-substrates, green malt supported higher maximum peak concentrations of C4, C5 and C6 under reducing conditions than rootlets while maintaining identical elongation kinetics and product selectivity.

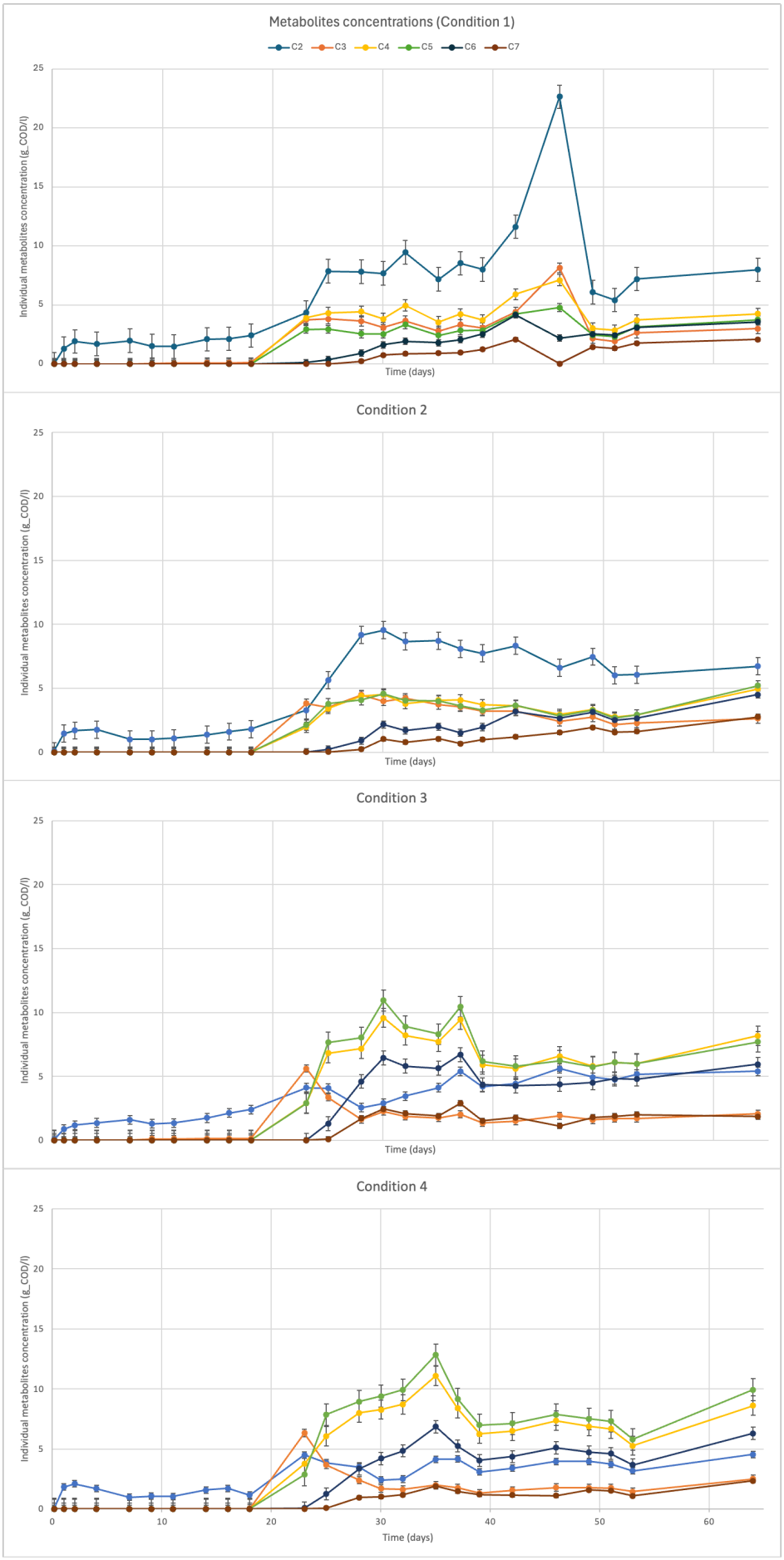
Metabolites concentrations (Condition 1)
C2
C3
C4
C5
C6
C7
Individual metabolites concentration (g_COD/l)
Time (days)
Condition 2
Individual metabolites concentration (g_COD/l)
Time (days)
Condition 3
Individual metabolites concentration (g_COD/l)
Time (days)
Condition 4
Individual metabolites concentration (g_COD/l)
Time (days)

Figure 14. Evolution of individual carboxylate concentrations (C_2 to C_7, expressed in g COD/L) over time across Conditions 1 to 4 (n = 3).

5.2.5 Normalized COD balance and organic fraction dynamics

The distribution of organic matter was tracked by comparing three distinct chemical oxygen demand (COD) fractions: Total COD representing the complete oxidizable matter in the mixed liquor (slurry including suspended solids and biomass), Soluble COD corresponding to the total dissolved organic fraction measured in the centrifuged supernatant, and total identified metabolites (Total) representing the sum of the theoretical COD of individually quantified carboxylates and alcohols. The difference between soluble COD and total identified metabolites represents the uncharacterized solubilized fraction (Unknown). The evolution of these fractions, along with cumulative net consumed H_2 and produced CH_4, is presented in Figure 15.

Total COD across Conditions 1, 3, and 4 followed a continuous, monotonic decrease from initial values of 70 kg COD/m^3r down to approximately 40 kg COD/m^3r at Day 64, reflecting regular mass removals from sampling. In Condition 2 (green malt under N_2), an initial step drop occurred between Day 0 and Day 1, before stabilizing along a parallel decrease down to 23 kg COD/m^3r. During the initial 20-day latency period, Soluble COD increased in all conditions from 12 to 20 kg COD/m^3r, driven entirely by non-fermentative substrate solubilization as identified metabolites remained below 3 kg COD/m^3r, resulting in a large accumulation of uncharacterized soluble intermediates.

Following microbial re-inoculation on Day 20 under N2 atmosphere (Conditions 1 and 2), this unknown soluble pool was rapidly consumed, falling below 5 kg COD/m^3r by Day 30 as identified metabolites accumulated to 22 kg COD/m^3r (dominated by SCCAs). In Condition 1, an analytical overestimation on Day 46 generated a transient artifact in total metabolites and a corresponding negative dip in unknown COD, which returned to baseline on Day 49. Net gaseous H_2 and CH_4 balances remained strictly zero under throughout the 64 days.

Under reducing atmosphere (Conditions 3 and 4), gaseous substrate consumption expanded the system's total COD capacity after Day 20, with cumulative consumed H_2 reaching +36 kg COD/m^3r in Condition 3 and +42 kg COD/m^3r in Condition 4 by Day 64. Total identified metabolites peaked between Days 32 and 35 (36 kg COD/m^3r in Condition 3; 38.5 kg COD/m^3r in Condition 4), with MCCAs accounting for 7.5-8.2 kg COD/m^3r. From Day 42 onward, the emergence of methanogenesis was reflected in the rapid drop of the net CH_4 curve (reaching -28.7 and -30.4 kg COD/m^3r, respectively). For Condition 4, soluble metabolite monitoring was halted at Day 53 due to data issues with the last two reactors.

Comparing co-substrates, green malt supported slightly higher peak metabolite accumulation (38.7 vs 36.2 kg COD/m^3r) and slightly higher net methane production under reducing conditions than rootlets, while exhibiting identical bioconversion trends and phase timing across all reactors.

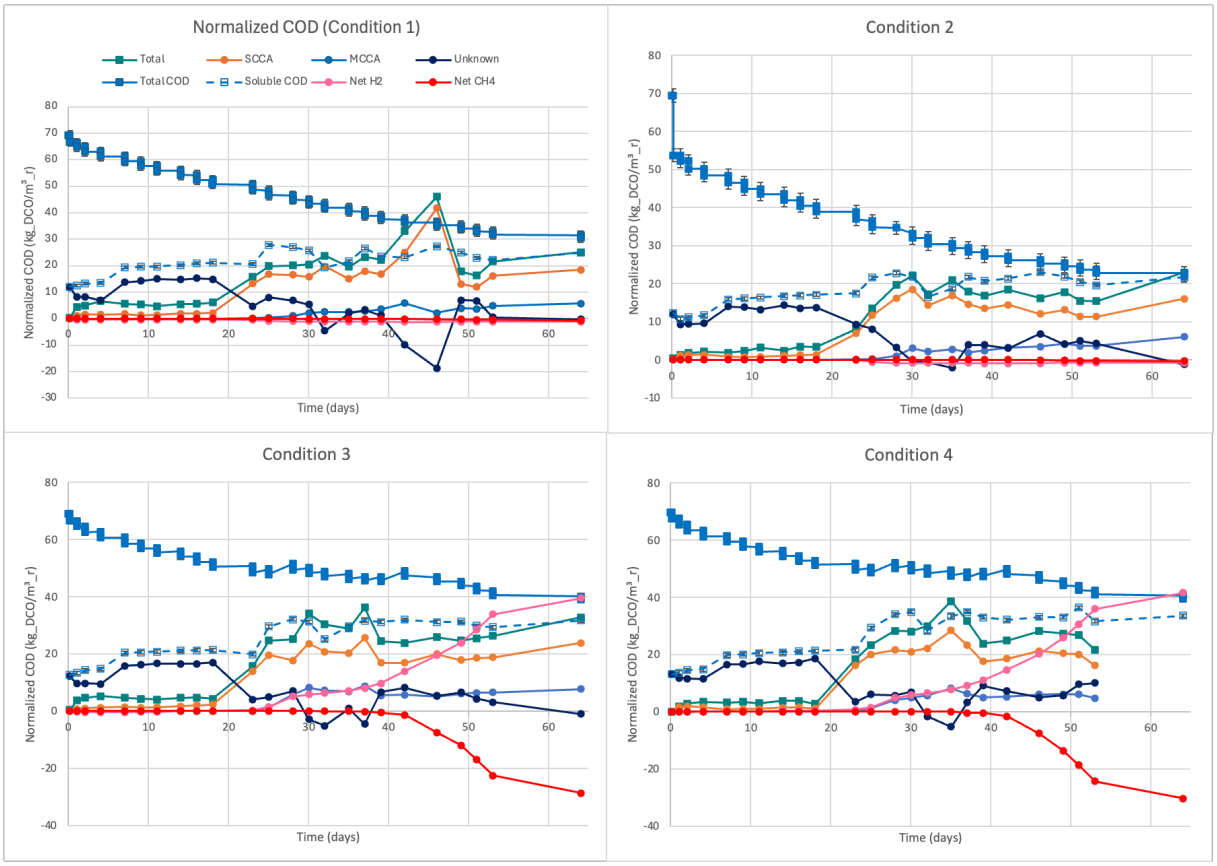

Figure 15. Evolution of normalized COD distribution over time across Conditions 1 to 4 (n = 3).

5.2.6 Cumulative end-point COD mass balance

The final cumulative COD mass balances comparing initial inputs (IN) and recovered product fractions (OUT) at the end of the fermentation are presented in Figure 16.

Under nitrogen atmosphere (Conditions 1 and 2), initial substrate input was identical at 16 g COD, consisting of orange peel waste and the respective co-substrate (rootlets or green malt). The total recovered product pool reached 6.9 g COD for rootlets (Condition 1) and 5 g COD for green malt (Condition 2). Recovered products were predominantly short-chain carboxylates, with SCCAs accounting for 4 g COD in Condition 1 and 3.6 g COD in Condition 2, while chain elongation to MCCAs remained modest (1.3 g COD). The uncharacterized soluble fraction (Unknown COD) stood at 1.4 g COD in Condition 1 and negative in Condition 2 which is an artefact, while gaseous products remained negligible.

Under reducing atmosphere (Conditions 3 and 4), total substrate input expanded to 25.1 g COD in Condition 3 and 25.3 g COD in Condition 4 due to substantial cumulative H_2 consumption. Correspondingly, the total recovered product pool more than doubled compared to N_2 atmosphere, reaching 15.5 g COD in Condition 3 and 15.7 g COD in Condition 4. Gaseous methane constituted the largest single product fraction. Carboxylate production remained sustained, with SCCAs yielding 5.3 g COD (Condition 3) and 4.7 g COD (Condition 4), while MCCAs reached 1.7 g COD and 1.6 g COD, alongside unknown soluble intermediates.

Comparing co-substrates, rootlets supported a slightly higher recovery of volatile fatty acids under both N_2 and H_2/CO_2.

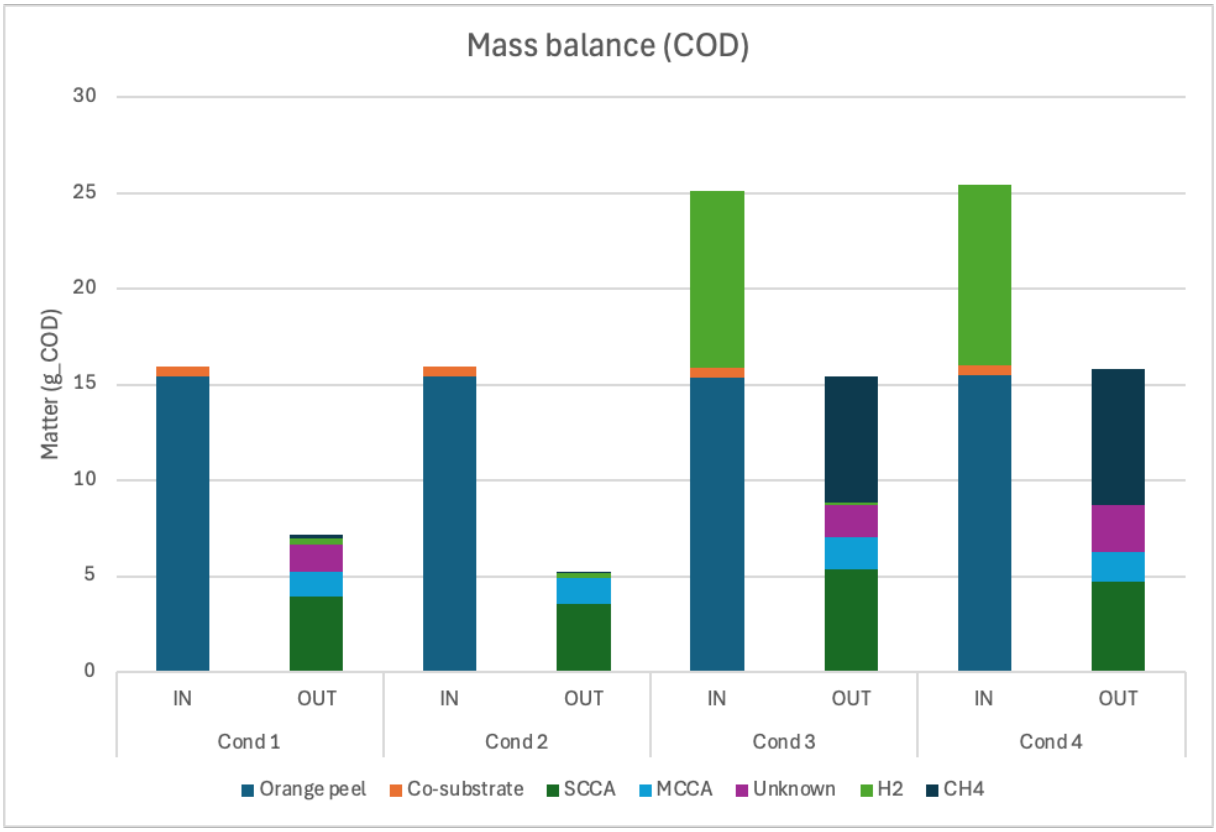

Figure 16. Final COD mass balances across Conditions 1 to 4 at the end of the fermentation. Values represent means of triplicates (n = 3) for Conditions 1, 2 and 3, and duplicate (n = 2) for 4 due to the exclusion of an outlier reactor. Co-substrates are distributed as rootlets – green malt – rootlets – green malt.

6 Discussion

6.1 Substrate biodegradability, initial acidification and D-Limonene inhibition

The initial stage of fermentation across all four reactors was characterized by an immediate drop in pH to 4.3 – 4.7 within the first 48 hours, followed by an extended 20-day latency period where volatile fatty acid synthesis remained arrested. This initial acidification reflects the rapid solubilization and primary acidogenesis of readily accessible free sugars and pectin monomers present in raw orange peels. However, the subsequent plateau in acidification and the stalling of carboxylate accumulation at residual acetate levels (1 – 2.4 g COD/L) between Days 2 and 20 highlight a bioenergetic and physiological inhibition.

As demonstrated in the normalized COD profiles, Soluble COD continued to increase during this latency phase (rising from 12 to 20 kg COD/m^3r) while identified carboxylates remained near zero, generating a substantial pool of uncharacterized soluble intermediates. This decoupling between polymer solubilization and fermentation confirms that hydrolytic dissolution proceeded, but downstream catabolic conversion was blocked.

This inhibition could be attributable to the essential oils naturally present in orange peel, composed of over 90% D-limonene (B. Ruiz and Flotats 2014). Due to its hydrophobic nature, D-limonene inserts into the lipid bilayer of microbial cell membranes, causing permeabilization, intracellular metabolite leakage, and the dissipation of the proton-motive force (PMF) required for ATP synthesis (Carneiro et al. 2020). While methanogens are particularly vulnerable to this steric disruption due to their ether-linked isoprenoid membrane architecture (Sikkema et al. 1995), the unadapted bacterial consortium in the return-activated sludge (RAS) also suffered transient metabolic arrest.

The microbial re-inoculation performed on Day 20 successfully relieved this bottleneck. Re-inoculation restored active biomass density after partial in situ volatilization and potentially

biotransformation of D-limonene into less toxic derivatives (such as terpineol and cymene) had taken place (Begoña Ruiz and Flotats 2016). Immediately following Day 20, the accumulated pool of uncharacterized soluble COD was rapidly consumed (falling below 5 kg COD/m^3r by Day 30), fuelling an immediate surge in carboxylate synthesis.

6.2 Influence of headspace composition on electron allocation

The reaction atmosphere exerted a decisive role in governing electron allocation, metabolic product selectivity, and carbon chain elongation kinetics.

Under an N_2 atmosphere (Conditions 1 and 2), the system operated as a classical acidogenic digestion. Acetate was the principal terminal metabolite (pic at 9.5 g COD/L), while chain elongation remained marginal, yielding only modest amounts of butyrate (5 g COD/L), valerate (3.5 – 5 g COD/L), and caproate (3.5 – 4.5 g COD/L). In the absence of an exogenous reduced electron donor, the direct condensation of acetate into elongated carboxylates is thermodynamically unfavourable for acetate reduction with H_2 (Agler et al. 2011). The system was thus bioenergetically trapped at the short-chain carboxylate stage.

Conversely, the exogenous supply of H_2/CO_2 (77/23% v/v) provided the necessary thermodynamic driving force to activate reductive pathways. Between Days 24 and 42, before the onset of methanogenesis, continuous gas consumption (+914 and 970 mol/m^3r of H_2) steered metabolic fluxes through two synergistic mechanisms: homoacetogenesis (Wood-Ljundahl) and rBOX chain elongation.

This gaseous electron influx altered the carboxylate profile in two fundamental ways:

Odd-Chain Elongation Dominance: Following re-inoculation, propionate (C3) peaked transiently (5.6 – 6.3 g COD/L) before being rapidly consumed down to < 2 g COD/L, exactly coinciding with the surge of valerate (C5) up to 11 – 12.8 g COD/L. This indicates that potentially, propionate acted as the primary electron-accepting primer, condensing with acetyl-CoA derived from homoacetogenesis to form odd-carbon chains (C3 $\rightarrow$ C5) via rBOX.

Enhanced Even-Chain Elongation: Concurrently, butyrate (C4) reached 9.6 – 11.1 g COD/L and caproate (C6) reached 6.7 g COD/L. The total recovered COD pool in the mass balance expanded from 5 – 6.9 g COD under N_2 to 15.5 – 15.7 g COD under H_2/CO_2, demonstrating that gaseous hydrogen was effectively fixed into soluble chemical energy.

6.3 Nutritional balancing and co-substrate synergy

Mono-fermentation of orange pulp is constrained by a nitrogen deficiency, characterized by a carbon-to-nitrogen (C/N) ratio exceeding 40:1 (characterized at 43.8 by Atelge, 2021). Such nitrogen limitation restricts microbial protein synthesis, cellular growth, and rBOX enzymatic expression (Liu et al. 2025).

Co-digestion with malting byproducts rebalanced the nutritional matrix without requiring synthetic ammonium supplementation. Both rootlets and green malt supplied bioavailable organic nitrogen (peptides, amino acids) and essential trace elements, potentially maintaining the fermentation in the C/N window (3 - 25) identified by Liu et al. (2025) to avoid both nitrogen starvation (C/N > 58) and hyper-ammoniacal toxicity.

Kinetic activation (green malt advantage): Green malt supported slightly faster initial gas consumption and higher peak concentrations of butyrate, valerate, and caproate under H_2/CO_2. This could be attributed to its high content of active hydrolytic enzymes (amylases, proteases) and readily soluble maltose/peptides, which accelerated metabolic startup post-re-inoculation.

Conversion completeness (rootlets advantage): Rootlets exhibited superior substrate conversion efficiency in the final mass balance. This could be because rootlets consist of dried, structural kilned proteins that release amino acids steadily without causing sudden nutrient surges, they sustained a higher total carboxylate yield (7.1 vs 6.2 g COD under reductive atmosphere).

6.4 The elongation window and process implications

The overarching objective of the carboxylate platform is to divert carbon and electrons away from low-value methane toward platform chemicals (Bastidas-Oyanedel and Schmidt 2018). A central finding of this study is the transient nature of the "methane-arrested" state when relying on endogenous substrate toxicity.

Between Days 20 and 42, methane production was completely suppressed, creating a productive 22-day elongation window where carboxylates accumulated up to 38.5 kg COD/m^3r. However, by Day 42, it seems that methanogenic archaea adapted to the residual terpene levels and rapidly colonized the system like already seen by Ruiz et al. (2014).

Once activated, hydrogenotrophic methanogens outcompeted homoacetogenic and elongating bacteria due to superior thermodynamic feasibility and higher substrate affinity (González-Cabaleiro et al. 2013). They acted as an aggressive "electron vacuum" (Agler et al. 2011).

Cumulative CH_4 production surged to -450 and -475 mol/m^3r, consuming over 44% of the total recovered COD pool in the mass balance.

Soluble carboxylate concentrations declined from their Day 35 peaks (C5 dropped from 12.8 to 7.7 g COD/L; C4 from 11.1 to 8.1 g COD/L), reflecting a potentially cessation of chain elongation and the possible secondary consumption of carboxylates by acetoclastic methanogens or syntrophic oxidizing consortia.

From a bioprocess engineering perspective, these findings define the operational limits of batch carboxylate production from citrus waste. While citrus essential oils provided an effective, chemical-free method to suppress methanogenesis during early fermentation, long-term operation could requires process interventions—such as harvesting the mixed liquor or initiating in situ membrane extraction (e.g., pertraction) precisely at the apex of the elongation

window (Days 32–35) before the methanogenic short-circuit depletes the carboxylate product pool.

7 Conclusion

This work evaluated the anaerobic fermentation of orange peel waste for carboxylate production using native sewage sludge, establishing how gaseous electron donors and nitrogenous co-substrates steer metabolic fluxes. The experimental results directly address the core research questions across four operational axes.

Orange peel waste underwent rapid initial acidification, followed by a 20-day latency phase where carboxylate production remained arrested. During this phase, hydrolytic solubilization continued generating a transient pool of uncharacterized soluble matter. The re-inoculation at Day 20 successfully unlocked the bioprocess following partial *in situ* volatilization and biotransformation of toxic D-limonene.

Under N_2, fermentation was thermodynamically confined to short-chain carboxylates dominated by acetate with minimal elongation. In contrast, exogenous H_2/CO_2 lifted the thermodynamic barrier via Wood-Ljungdahl homoacetogenesis and reverse rBOX. Gaseous consumption fuelled odd-chain elongation (C3 $\rightarrow$ C5) surging valerate to 12.8 g COD/L alongside butyrate (11.1 g COD/L) and caproate (6.7 g COD/L), effectively more than doubling the recovered COD mass balance to 15.5 – 15.7 g COD.

Both malting residues rebalanced the initial carbon-to-nitrogen ratio without requiring synthetic ammonium. Green malt provided slightly superior kinetic activation, accelerating initial gas uptake and delivering higher peak carboxylate concentrations, possibly due to accessible hydrolytic enzymes and soluble sugars. Conversely, rootlets promoted greater conversion completeness in the end-point mass balance, achieving higher total carboxylate recovery.

Endogenous D-limonene toxicity provided a chemical-free, 22-day elongation window (Days 20–42) with zero methane emissions. However, by Day 42, microbial adaptation enabled hydrogenotrophic methanogens to recover. These archaea acted as an aggressive "electron vacuum," consuming over 44% of the total recovered COD pool and triggering the degradation of accumulated carboxylates.

It must be noted that at the time of finalizing this thesis, high-throughput sequencing data from the extracted genomic DNA remained pending from an external analytical laboratory. Consequently, community structure, guild succession, and taxonomic shifts were not defined and must be determined by future investigations.

Building upon these findings, future research should primarily focus on integrating the forthcoming sequencing datasets to formally validate taxonomic guild successions, and hydrogenotrophic archaea across the different metabolic phases. To prevent carboxylate loss following the Day 42 methanogenic shift, bioprocess development should prioritize coupling reactors with *in situ* product recovery systems (such as membrane pertraction) timed precisely at the apex of the elongation window. Furthermore, transitioning toward a continuous two-stage configuration could decouple orange hydrolysis and controlled D-limonene dosing from the elongation stage, enabling sustained, chemical-free methanogenic suppression over long operational horizons. Finally, addressing gas-liquid mass transfer limitations via hollow-fiber membrane contactors or micro-sparging systems would increase dissolved H_2 availability, accelerating reverse β-oxidation kinetics before archaeal adaptation can take place.

8 Bibliography

Agler, Matthew T., Brian A. Wrenn, Stephen H. Zinder, and Largus T. Angenent. 2011. 'Waste to Bioproduct Conversion with Undefined Mixed Cultures: The Carboxylate Platform'. *Trends in Biotechnology* 29 (2): 70–78. https://doi.org/10.1016/j.tibtech.2010.11.006.

Angelidaki, Irini, Laura Treu, Panagiotis Tsapekos, et al. 2018. 'Biogas Upgrading and Utilization: Current Status and Perspectives'. *Biotechnology Advances* 36 (2): 452–66. https://doi.org/10.1016/j.biotechadv.2018.01.011.

Angenent, Largus T., Hanno Richter, Wolfgang Buckel, et al. 2016. 'Chain Elongation with Reactor Microbiomes: Open-Culture Biotechnology To Produce Biochemicals'. *Environmental Science & Technology* 50 (6): 2796–810. https://doi.org/10.1021/acs.est.5b04847.

Atelge, Rasit. 2021. 'Co-Digestion of Orange Pulp and Cattle Manure with Different C/N Ratios and A New Modeling of Biogas Production'. *Karadeniz Fen Bilimleri Dergisi* 11 (December): 557–69. https://doi.org/10.31466/kfbd.937269.

Bastidas-Oyanedel, Juan-Rodrigo, and Jens Ejbye Schmidt. 2018. 'Increasing Profits in Food Waste Biorefinery—A Techno-Economic Analysis'. *Energies* 11 (6): 1551. https://doi.org/10.3390/en11061551.

Battista, Federico, Gianmarco Remelli, Serena Zanzoni, and David Bolzonella. 2020. 'Valorization of Residual Orange Peels: Limonene Recovery, Volatile Fatty Acids, and Biogas Production'. *ACS Sustainable Chemistry & Engineering* XXXX (April). https://doi.org/10.1021/acssuschemeng.0c01735.

Carneiro, Victor Alves, Ramaiana Soares Melo, Antônio Mateus Gomes Pereira, et al. 2020. 'Essential Oils as an Innovative Approach against Biofilm of Multidrug-Resistant Staphylococcus Aureus'. In *Bacterial Biofilms*. IntechOpen. https://doi.org/10.5772/intechopen.91833.

González-Cabaleiro, Rebeca, Juan M. Lema, Jorge Rodríguez, and Robbert Kleerebezem. 2013. 'Linking Thermodynamics and Kinetics to Assess Pathway Reversibility in Anaerobic Bioprocesses'. *Energy & Environmental Science* 6 (12): 3780–89. https://doi.org/10.1039/c3ee42754d.

Grootscholten, T. I. M., D. P. B. T. B. Strik, K. J. J. Steinbusch, C. J. N. Buisman, and H. V. M. Hamelers. 2014. 'Two-Stage Medium Chain Fatty Acid (MCFA) Production from Municipal Solid Waste and Ethanol'. *Applied Energy* 116 (March): 223–29. https://doi.org/10.1016/j.apenergy.2013.11.061.

Henry, Grégoire B. L., Florent Awedem Wobiwo, Arnaud Isenborghs, et al. 2023a. 'A Specific H2/CO2 Consumption Molar Ratio of 3 as a Signature for the Chain Elongation of Carboxylates from Brewer's Spent Grain Acidogenesis'. *Frontiers in Bioengineering and Biotechnology* 11 (June). https://doi.org/10.3389/fbioe.2023.1165197.

Henry, Grégoire B. L., Florent Awedem Wobiwo, Arnaud Isenborghs, et al. 2023b. 'A Specific H2/CO2 Consumption Molar Ratio of 3 as a Signature for the Chain Elongation of Carboxylates from Brewer's Spent Grain Acidogenesis'. *Frontiers in Bioengineering and Biotechnology* 11 (June). https://doi.org/10.3389/fbioe.2023.1165197.

Holtzapple, Mark T., and Cesar B. Granda. 2009. 'Carboxylate Platform: The MixAlco Process Part 1: Comparison of Three Biomass Conversion Platforms'. *Applied Biochemistry and Biotechnology* 156 (1): 95–106. https://doi.org/10.1007/s12010-008-8466-y.

Kleerebezem, Robbert, and Mark CM van Loosdrecht. 2007. 'Mixed Culture Biotechnology for Bioenergy Production'. *Current Opinion in Biotechnology*, Energy biotechnology / Environmental biotechnology, vol. 18 (3): 207–12. https://doi.org/10.1016/j.copbio.2007.05.001.

Liu, Longlong, Yingmeng Shen, Sen Yang, Zhengang Chen, Xiaofeng Ji, and Jiying Zhu. 2025. 'Optimizing Caproic Acid Biosynthesis in Anaerobic Fermentation of Ethanol and Butanoic Acid: The Effects of C/N Ratio'. *Fermentation* 11 (6): 316. https://doi.org/10.3390/fermentation11060316.

Nzeteu, Corine Orline, Anna Christine Trego, Florence Abram, and Vincent O'Flaherty. 2018. 'Reproducible, High-Yielding, Biological Caproate Production from Food Waste Using a Single-Phase Anaerobic Reactor System'. *Biotechnology for Biofuels* 11 (1): 108. https://doi.org/10.1186/s13068-018-1101-4.

Ruiz, B., and X. Flotats. 2014. 'Citrus Essential Oils and Their Influence on the Anaerobic Digestion Process: An Overview'. *Waste Management* 34 (11): 2063–79. https://doi.org/10.1016/j.wasman.2014.06.026.

Ruiz, Begoña, and Xavier Flotats. 2016. 'Effect of Limonene on Batch Anaerobic Digestion of Citrus Peel Waste'. *Biochemical Engineering Journal* 109 (May): 9–18. https://doi.org/10.1016/j.bej.2015.12.011.

Seedorf, Henning, W. Florian Fricke, Birgit Veith, et al. 2008. 'The Genome of Clostridium Kluyveri, a Strict Anaerobe with Unique Metabolic Features'. *Proceedings of the National Academy of Sciences* 105 (6): 2128–33. https://doi.org/10.1073/pnas.0711093105.

Sikkema, J., J. A. de Bont, and B. Poolman. 1995. 'Mechanisms of Membrane Toxicity of Hydrocarbons'. *Microbiological Reviews* 59 (2): 201–22. https://doi.org/10.1128/mr.59.2.201-222.1995.

Spirito, Catherine M., Hanno Richter, Korneel Rabaey, Alfons JM Stams, and Largus T. Angenent. 2014. 'Chain Elongation in Anaerobic Reactor Microbiomes to Recover Resources from Waste'. *Current Opinion in Biotechnology*, Energy biotechnology • Environmental biotechnology, vol. 27 (June): 115–22. https://doi.org/10.1016/j.copbio.2014.01.003.

Stamatopoulou, Panagiota, Juliet Malkowski, Leandro Conrado, Kennedy Brown, and Matthew Scarborough. 2020. 'Fermentation of Organic Residues to Beneficial

Chemicals: A Review of Medium-Chain Fatty Acid Production'. *Processes* 8 (12): 1571. https://doi.org/10.3390/pr8121571.

Steinbusch, Kirsten J. J., Hubertus V. M. Hamelers, Caroline M. Plugge, and Cees J. N. Buisman. 2011. 'Biological Formation of Caproate and Caprylate from Acetate: Fuel and Chemical Production from Low Grade Biomass'. *Energy & Environmental Science* 4 (1): 216–24. https://doi.org/10.1039/c0ee00282h.

Wasajjaa, Henry, Ralph E. F. Lindeboom, Jules B. van Lier, and P. V. Aravind. 2020. 'Techno-Economic Review of Biogas Cleaning Technologies for Small Scale off-Grid Solid Oxide Fuel Cell Applications'. *Fuel Processing Technology* 197 (106215). https://doi.org/10.1016/j.fuproc.2019.106215.

Zhang, Cunsheng, Hongze Liu, Min Li, Shuhao Huo, Qingyan Wang, and Akram Avami. 2026. 'Production of Medium-Chain Carboxylic Acids via Chain Elongation: Challenges, Strategies, and Perspectives'. *Journal of Agricultural and Food Chemistry* 74 (6): 4915–32. https://doi.org/10.1021/acs.jafc.5c05195.

Methane-arrested anaerobic fermentation of orange peel waste: impact of headspace gas composition and nitrogenous co-Substrates on carboxylate Profiles

Mathis Herbin

Within the transition toward a circular bioeconomy, the carboxylate platform provides a "Waste-to-Chemicals" route to convert agro-industrial residues into high-value platform molecules, particularly medium-chain carboxylic acids (MCCAs) via anaerobic chain elongation (rBOX). However, the anaerobic valorisation of orange peel waste faces two major hurdles: a nitrogen deficiency and the antimicrobial toxicity of endogenous essential oils, predominantly D-limonene.

This master's thesis aims to evaluate and optimize the anaerobic fermentation of orange peel waste inoculated with sewage sludge, investigating how the combination of nitrogenous malting co-substrates and headspace gas control can overcome bioenergetic barriers, suppress methanogenesis naturally, and selectively steer metabolic fluxes toward elongated carboxylates.

Batch anaerobic fermentations of orange peel pulp were carried out over 64 days using native municipal return activated sludge. Two industrial malting residues (rootlets vs green malt) were evaluated as co-substrates under two contrasting headspace atmospheres: a nitrogen control versus a reducing hydrogen/carbon dioxide mixture. Process performance was monitored through periodic pH regulation, headspace gas composition profiling, chromatographic quantification of soluble carboxylates, and cumulative COD mass balances.

Endogenous D-limonene from orange peel waste naturally arrested methanogenesis, securing a productive, chemical-free window that enabled carboxylate accumulation following re-inoculation. While a N_2 atmosphere remained thermodynamically restricted to short-chain acids, supplying an H_2/CO_2 headspace overcame this bioenergetic bottleneck, driving homoacetogenesis and reverse β-oxidation to selectively boost valerate, butyrate, and caproate synthesis. Malting by-products effectively rebalanced the C/N ratio without synthetic additives, where green malt accelerated initial startup kinetics while rootlets ensured superior conversion completeness in the final mass balance. However, the late-stage recovery of hydrogenotrophic methanogens acted as an electron vacuum that depleted carboxylate yields. Integrating pending metagenomic sequencing data could validate the functional succession of key elongating guilds and archaea.

UNIVERSITÉ CATHOLIQUE DE LOUVAIN
Faculté des bioingénieurs
Croix du Sud, 2 bte L7.05.01, 1348 Louvain-la-Neuve, Belgique | **www.uclouvain.be/agro**